Cool Flame Combustion Experiment (*Cool Combustion*, CFI)

A **Science Requirements Document (SRD)** submitted to
The National Aeronautics and Space Administration

November 7, 2014

Forman A. Williams
University of California, San Diego

.....

Signature

.....

Date

Frederick L. Dryer
Princeton University

.....

Signature

.....

Date

Tanvir Farouk
University of South Carolina

.....

Signature

.....

Date

Vedha Nayagam
Case Western Reserve University

.....

Signature

.....

Date

Daniel L. Dietrich
NASA Glenn Research Center

.....

Signature

.....

Date

Andrew C. Suttles, Project Manager
NASA Glenn Research Center

.....

Signature

.....

Date

Francis P. Chiaramonte, Program Scientist
NASA Headquarters

.....

Signature

.....

Date

Contents

1 Introduction **8**

2 Background **10**
2.1 Low Temperature Chemical Kinetics . . . 10
2.2 Microgravity Droplet Combustion . . . 11
2.3 The FLEX Experiments . . . 12
2.3.1 Experiment Hardware . . . 12
2.3.2 Experiment Diagnostics . . . 13
2.3.3 Data Analysis . . . 14
2.3.4 Cool Flame Burning Mode . . . 17
2.4 Summary of FLEX Cool Flame Experiments to Date . . . 20
2.4.1 Cool flames are prevalent . . . 21
2.4.2 Significant effect of ambient pressure . . . 23
2.4.3 The effect of ambient gas composition . . . 25
2.4.4 The effect of fuel composition . . . 26
2.5 Summary . . . 26

3 Experiment Objectives **30**
3.1 Objectives of the proposed effort . . . 30
3.2 Fuel . . . 30
3.2.1 Baseline Fuel . . . 30
3.2.2 Isomeric Fuels and Surrogate Fuel Blends . . . 31
3.2.3 Fuel Additive . . . 31
3.3 Ambient Conditions . . . 31

4 Microgravity Justification **33**

5 Science Requirements **35**
5.1 Experiment Requirements . . . 35
5.1.1 Test Fuels . . . 36
5.1.2 Droplet Deployment and Ignition . . . 37
5.1.3 Initial Pressure . . . 37
5.1.4 Initial Ambient . . . 37
5.1.5 Misc. Ambient Requirements . . . 38
5.1.6 Operational Requirements . . . 38
5.1.7 Microgravity Requirements . . . 38
5.2 Diagnostic Requirements . . . 39
5.2.1 Droplet Imaging . . . 41
5.2.2 $OH*$ or CH Hot-Flame Imaging . . . 41
5.2.3 CH_2O Cool-Flame Imaging . . . 42
5.2.4 Secondary Color Flame Imaging . . . 43
5.2.5 Flame Radiation . . . 43
5.2.6 Fiber/Flame Temperature . . . 44
5.2.7 Ambient Temperature and Pressure Measurement . . . 44
5.2.8 Synchronization . . . 44

6 Test Matrix and Experiment Procedure **45**
6.1 Flight Experiment Test Procedures 45
6.2 FLEX Test Matrix 46

7 Success Criteria **47**
7.1 Minimal Success 47
7.2 Complete Success 47

8 Data Requirements **48**
8.1 Temporal Droplet History 48
8.2 Flame Shape and Structure 48
8.3 Flame Radiation 49

9 Principal Deliverables **49**

List of Figures

1 Schematic of the Multi-user Droplet Combustion Apparatus (MDCA). This is altered for clarity and is not the exact layout of the MDCA. 13

2 FLEX image sequence for a heptane droplet from the three cameras corresponding to the times denoted by the dashed lines in the subsequent figure. The left column is from the HiBMS camera, the center column from the LLUV camera and the right column from the color camera. The ambient oxygen and nitrogen mole fractions were 0.18 and 0.72, respectively and the ambient pressure was 1.0 atm. 15

3 Droplet and flame histories for the heptane droplet in Fig. 2, initially 3.41 mm in diameter. The ambient environment had oxygen and nitrogen mole fractions of 0.18 and 0.72, respectively and a pressure of 1.0 atm. The gap in the droplet history at $t/D_0^2 \sim 1.5$ is when the droplet drifted out of the field of view of the HiBMS camera (the drift velocity was on the order of 1 - 2 mm/s). The thin vertical lines with letters correspond to the different times of the image sequence in Fig. 2. The thick dashed vertical line (coincident to when the flame diameter and standoff decrease quickly) is when visible flame extinction occurred. 16

4 Droplet and flame histories for two heptane droplets ($D_0 = 2.1$, $3.0\,mm$) burning in a 0.20/0.75/0.05 $O_2/N_2/CO_2$, $1.0\,atm$ ambient environment. The flame is that measured by the LLUV. The smaller droplet drifted out of the field of view before the end of the test. The vertical dashed lines indicate the time where flame extinction occurred; the dashed line at 20+ s marks the approximate time of the second extinction. For clarity, the graphs show a subset (one of every five) of the experimental data. 18

5 Experimental (FLEX) and predicted (Farouk and Dryer, 2014) droplet and flame histories for a heptane droplet ($D_0 = 3.9\,mm$) burning in a nominally air (0.21 oxygen mole fraction, balance nitrogen), 1.0 atm ambient environment. The numerical predictions contain both high and low temperature chemistry. For clarity, the graphs show a subset (one of every ten for the droplet, one of every five for the flame) of the experimental data. 19

6 The droplet, flame and radiometer histories for a heptane droplet ($D_0 = 3.61\,mm$) burning in a nominally air (0.21 oxygen mole fraction, balance nitrogen), 1.0 atm ambient environment. The droplet diameter and time are both normalized by the initial droplet diameter squared. The narrowband flame radiance is scaled by a factor of 10 to put it on the same scale as the wideband flame radiance. 22

7 The droplet, flame and radiometer histories for two decane droplets burning in a 0.21 ambient oxygen mole fraction (balance nitrogen) environment and 0.50 and 1.0 atm pressure. The droplet diameter and time are both normalized by the initial droplet diameter squared. The narrowband flame radiance is scaled by a factor of 10 to put it on the same scale as the wideband flame radiance. 24

8 The droplet, flame and radiometer histories for a heptane droplets burning in a 0.21 ambient oxygen mole fraction (0.30 nitrogen and 0.50 carbon dioxide) environment and 3.0 atm pressure. The droplet diameter and time are both normalized by the initial droplet diameter squared. 25

9 The droplet, flame and radiometer histories for n-octane droplets burning in a 0.21 ambient oxygen mole fraction at 1.0 *atm* pressure. The diluent gases in the two tests were nitrogen/helium mixtures with helium mole fractions (balance nitrogen) of 0.15 and 0.50. The narrowband radiometer is scaled by a factor of 10 so it can appear on the same scale as the wideband data. 27
10 The droplet, flame and radiometer histories for heptane/ethanol droplet burning in a nominally air 0.21/0.79 oxygen/nitrogen, 1.0 *atm*) ambient environment. The narrowband radiometer is scaled by a factor of 10 so it can appear on the same scale as the wideband data. 28
11 Chemiluminescence spectra from excited formaldehyde (Sheinson and Williams, 1973). 42

List of Tables

1 Hardware requirements tabulation. 35
2 Diagnostic requirements tabulation. 40
3 Nominal test matrix for n-dodecane. The droplet size range for the tests is 2 - 6 mm. 46
4 Nominal test matrix for the other fuels and fuel mixtures. The droplet size range for the tests is 2 - 6 mm. 47

1 Introduction

Understanding the combustion characteristics of liquid hydrocarbon fuels is of practical and fundamental importance. The United States alone consumes approximately 19 million barrels of liquid fuels per day which averages out to an astonishing 2.5 gallons per day per person (Reitz, 2013). The primary reasons for such a high reliance on hydrocarbon fuels as the single most important energy source, not only in the US but globally, is their high energy density, ease of handling, and portability compared to many other forms of energy. With the emergence of newer internal combustion engine technologies such as Homogeneous Charge Compression Ignition (HCCI) and Reactivity-Controlled Compression Ignition (RCCI) engines, understanding the autoignition and heat release chemistry and kinetics of hydrocarbon fuels is more important that ever. These new technologies coupled with the emergence of major sources of renewable fuels for both gasoline and diesel applications, including butanols and heavier alcohols, bio-diesel, farnesane and high carbon number synthetics, further emphasize the need to understand the kinetic effects of blending renewables with petroleum derived fuels.

Commercially available transportation fuels, such as gasoline, diesel, and jet fuel, are comprised of many hydrocarbon compounds, normal alkanes and branched alkanes being the major components. The combustion characteristics of these alkanes are quite complex and follow branched chain reaction pathways involving many (hundreds) intermediate radicals. The chemical pathways vary depending on temperature and to a lesser extent on pressure. Researchers typically identify a low temperature reaction mechanism and a high temperature mechanism, as well as a region of transition between the two (intermediate or transition). Many hydrocarbons exhibit a unique feature in the transition region where the reaction rate first decreases with increasing temperature (the negative temperature coefficient, NTC region). The NTC region precedes a region in which the reaction auto-accelerates to the high temperature region. Cool flames and the associated multi-stage ignition phenomenon occur as a result of the low, NTC, and hot ignition behavior of the fuels. In spark ignition engines, these chemistries are responsible for engine *knock*. The resistance of the fuel to *knock* is frequently characterized by the fuel's octane Number (ON); the higher the ON the less prone the engine is to *knock*.

The same low temperature chemistry controls the autoignition process in Compression Ignition (e.g., diesel) engines. The two stage autoignition process defines when combustion occurs and is typically characterized by a fuel's cetane number (CN); the more prone the fuel to autoignite, the higher the CN.

Researchers have applied a number of experimental techniques to investigate the chemical kinetic mechanisms that result in cool flame phenomena and thus control a fuel's ON/CN. These facilities include stirred reactors, flow reactors, shock tubes, rapid compression machines, and burner-stabilized two stage laminar flames. All these studies primarily involve premixed gases and attempt to understand the ignition process and transition from the low temperature region, through the intermediate temperature region to the high temperature, explosively branched region.

Droplet combustion experiments conducted onboard the International Space Station (ISS), as part of the Flame Extinguishment Experiment (FLEX) revealed conclusively for the first time that the combustion of large alkane droplets can exhibit a lengthy unique burning behavior as a result of this complex chemistry. After ignition, and high temperature burning and radiative flame extinction, large n-alkane droplets burn quasi-steadily in the low-temperature regime, characterized by NTC chemistry (Nayagam et al., 2012). This cool flame combustion ends abruptly at a finite droplet diameter, leaving the unvaporized droplet in the hot ambient. These observations provide a new, exciting and unique experimental configuration to further explore these chemical kinetic transitions, especially the low temperature chemistry of liquid fuels. Though this type of burning

behavior is likely to have been present (but not observed or reported) in prior droplet combustion research, the conditions of the FLEX experiments are such that the data have provided a wealth of detail with regard to this phenomena. The cool flame droplet burning rates provide a measure of the chemical heat release rate, the flame diameter (both hot and cool flame diameter) evolution provides insight into the effects of diffusive/convective/radiative heat loss, and the transitions in droplet high/low temperature burning/extinction provide stringent characterization of chemical kinetic behavior through their associated characteristic times.

The overall objective of this proposed research is to conduct further systematic experimental measurements of large droplets that exhibit the cool flame mode of combustion using the Multiuser Droplet Combustion Apparatus (MDCA) currently installed in the Combustion Integrated Rack (CIR) on the International Space Station (ISS). The experiments will examine the hot/cool flame behavior of a range of fuels in varied ambient environments (diluent/oxidizer composition and ambient pressure). Numerical simulations with detailed chemical kinetic models and theoretical analyses with reduced kinetics will complement the experiments with the ultimate goal to improve and validate the chemical kinetic models.

The science team anticipates that these studies will directly impact many potential applications on earth. The next generation piston engine technologies will benefit from the improved understanding of the chemical reactivity of fuels, as these properties are essential in controlling HCCI engines. RCCI engines efficiencies are as much as 40% greater than today's spark ignition and diesel designs. They have already been demonstrated in the laboratory, with such low NO_x and particulate emissions that no emissions after-treatment is necessary. Achieving a more appropriate means of varying the reactivity behavior of the fuels is necessary to realize the true potential of these discoveries. Detonation engines, an innovative means of generating high propulsive thrust, can also be improved and better controlled by understanding the same complex chemistries described above. Other terrestrial applications include fuel reformulation and production of hydrogen from gasoline for use in fuel cells (Naidja et al., 2003). Another area of application is fire safety in space vehicles. Since the cool flame mode of droplet combustion can persist after hot-flame extinction (and may even transition back to hot flaming under certain conditions), safety procedures based only on considerations of hot flame properties or sensing may be inadequate for assuring safety under all conditions.

2 Background

2.1 Low Temperature Chemical Kinetics

Traditionally cool flames are associated with premixed combustion that lead to multi-stage ignition of some fuels under certain pressure and temperature conditions. Though the existence of cool flames has been known since the days of Sir Humphry Davy (1817), Perkin (1882) was the first to conduct systematic studies and classified a range of organic compounds including alcohol, aldehydes, acids, oils, and waxes that can support cool flames. The study of cool flames, however, remained more of a scientific curiosity, because of its unusual oscillatory characteristics in a homogeneous medium, rather than of any practical interest. Researchers proposed non-linear theoretical models based on "isothermal" kinetics to explain the periodic cool flame oscillations; including the one by Frank-Kamenetskii and Thon (1955) based on the Lotka-Volterra equation. Salnikoff was the first to propose a "thermo-kinetic" theory where thermal feedback played a role in intermediate species production rate with a simple scheme:

$$A \xrightarrow{k1} X \xrightarrow{k2} B. \tag{1}$$

Salnikoff's theory, however, failed to explain many aspects of cool flame phenomenon including the negative temperature coefficient region. Yang and Gray (1969) proposed a more satisfactory thermokinetic scheme.

$$A \xrightarrow{k1} X \qquad \text{(initiation)} \tag{2}$$

$$X \xrightarrow{kb} 2X \qquad \text{(branching)} \tag{3}$$

$$X \xrightarrow{kt1} \text{stable products} \qquad \text{(low-temperature termination)} \tag{4}$$

$$X \xrightarrow{kt2} \text{stable products} \qquad \text{(high-temperature termination)} \tag{5}$$

They showed that for this scheme the NTC region is possible when the activation energies obey the following condition:

$$E_{t1} < E_b < E_{t2}. \tag{6}$$

With a set of assumed rate constants they were able to demonstrate many features of hydrocarbon oxidation including explosion limits, cool flame oscillation limits, oscillation amplitude and period, and the NTC region. Wang and Mou (1985) proposed improvements to the Gray-Yang model that includes an additional intermediate species that accounts for fuel consumption. Recently, Foster and Pearlman (2012) used this scheme to model unstirred static reactors with coupled species and thermal diffusion as well as buoyancy induced flows. Their numerical predictions compare qualitatively with experiments carried out microgravity and normal gravity for cool flame oscillations and ignition times (Pearlman, 2000; Fairlie et al., 2005). While these simplified reaction schemes provide a conceptual framework to understand the complex hydrocarbon oxidation processes, they are not very useful for quantitative prediction of the combustion characteristics of practical liquid fuels.

Modern studies of hydrocarbon oxidation involve developing detailed multi-step chemical kinetic schemes based on large number of elementary reactions that vary with pressure and temperature. The rate parameters associated with these elementary reactions are either from experiments or calculated from fundamental quantum mechanical theories such as transition state theory. Obtaining accurate rate parameters, however, is often difficult as they can contain large uncertainties. Over the past several decades a number of detailed chemical kinetic mechanisms have become available, notably those for n-alkanes (Curran et al., 1998, 2002; Ranzi et al., 1995, 2005; Biet et al.,

2008). The construction of the detailed mechanisms is based on the authors' long experience in the field, the systematic classification of possible reaction types and similarity to simpler submodels for smaller molecules ($C_0 - C_4$) for which the number of elementary reactions are minimal (e.g., Curran et al., 1998). In some cases the detailed chemical mechanisms have been, in part, constructed using automation software (e.g. EXGAS, Buda et al., 2005), Rapid Mechanism Generator (RMG, Harper et al., 2011) or other software based methods to apply parameter generation based upon families of reaction types.

While the detailed mechanisms provide information on many aspects of the reacting system such as product speciation, temperature, ignition times, flame propagation speeds, etc., they are not directly applicable for incorporation into computer models of practical combustion systems that involve complex flow geometries, time dependence and turbulence. Researchers in the past have developed techniques to systematically reduce the number of reaction steps and species needed from the detailed mechanisms to capture the salient features of the combustion processes both in the low temperature and high temperature regimes (Griffiths, 1995; Peters et al., 2002; Prince and Williams, 2012). In some instances semi-empirical methods have been used to generate one or two step global reaction models applicable to high temperature combustion (Westbrook and Dryer, 1981).

Detailed chemical kinetic mechanisms are typically validated using a variety of experimental techniques including shock tubes (Smith et al., 2005; Davidson et al., 2008), rapid compression engines (Tanaka et al., 2003), stirred and flow reactors (Held et al., 1997), premixed flames (El Bakali et al., 1999), diffusion flames (Seiser et al., 2000), and to a lesser extent with droplet flames (Nayagam et al., 1998; Marchese et al., 1999b; Tanabe et al., 1996). Each of these experimental techniques has their own limitations and advantages. In terrestrial laboratories, virtually all of the experimental techniques are influenced, to some extent, by multi-dimensional spatial and time dependent nature of the combustion process (e.g., ignition) itself. Such experiments are very difficult to model time dependently in terms of fully detailed chemical kinetics that include low, intermediate and high temperature kinetics, including fundamental diffusive/convective coupling and energy balance (Chaos and Dryer, 2008). Spherical symmetric single droplet burning of an isolated fuel droplet in microgravity provides a unique experimental means of testing and validating detailed and reduced chemical kinetic schemes in a simplified geometric configuration that includes detailed effects of diffusion, convection, chemical reaction, and heat coupling with the surrounding environment..

2.2 Microgravity Droplet Combustion

For over 50 years, scientists have been studying droplet combustion in microgravity, beginning with the modest one-second drop-tower experiments by (Kumagai, 1956) and including space experiments conducted onboard the NASA's Space Shuttle (Dietrich et al., 1996; Nayagam et al., 1998). Researchers exploit the spherically symmetric, one-dimensional burning of liquid fuel droplets in microgravity as a means to study the combustion characteristics of liquid fuels in a controlled fashion that is amenable to detailed numerical modeling and theoretical analyses. Past studies include many aspects of liquid fuel combustion including burning rates, flame dynamics, soot formation, multi-component effects, and ignition and extinction characteristics under various ambient conditions using microgravity droplet combustion experiments (e.g., Faeth, 1977; Law, 1982; Sirignano, 1983; Choi and Dryer, 2001)).

The conventional wisdom until recently has been that small hydrocarbon fuel droplets, once ignited, either burn to completion, extinguish in a flash as consequence of impurity or product accumulation, or extinguish diffusively (Law, 1975) at a finite droplet diameter. This diffusive ex-

tinction occurs when the diffusion time, which decreases with decreasing droplet diameter, becomes less than the chemical time required to complete the heat release in the gas phase. In microgravity where the buoyancy-induced flow is absent, larger droplets can extinguish as a result of the excessive radiant heat loss from the flame zone (Chao et al., 1991). This radiative extinction occurs because as the droplet diameter increases, the rate of radiant loss (proportional to the flame volume) increases faster than the rate of heat release (proportional to the droplet diameter). Following either one of these two modes of extinction, the droplet simply evaporates in the hot environment, without any chemical heat release in the gas phase. Theoretical models (e.g., Chao et al., 1991; Card and Williams, 1992b,a) and numerical simulations (e.g., Marchese et al., 1999a) with detailed high temperature chemical kinetics support this understanding.

2.3 The FLEX Experiments

2.3.1 Experiment Hardware

The ISS provides almost limitless microgravity time for combustion science research. The Flame Extinguishment Experiment (FLEX) is the first experiment in the multi-purpose combustion facility developed at the NASA Glenn Research Center (GRC). The Combustion Integrated Rack (CIR) provides the combustion chamber, most of the diagnostics, gas mixing system and the primary interface between the ISS and the ground controllers at NASA GRC. The Multi-User Droplet Combustion Apparatus (MDCA), inserted into the CIR, is the hardware that deploys and ignites the liquid fuel droplets. It communicates through the CIR to ground controllers at NASA GRC.

The CIR facility, occupying a large rack in the Destiny module of the ISS and described in detail elsewhere (Banu, 2008), consists of a 90 l combustion chamber that is capable of operating pressures of approximately 0 - 9 atm. The maximum pressure for a given experiment is frequently much less than 9 atm depending on a rigorous (and very conservative) safety analysis. For the FLEX experiments, this analysis reduced the maximum working pressures to approximately 3 atm. The interior of the CIR chamber contains the mechanical, fluid and electrical interfaces necessary to mount experiment-specific hardware inside the chamber.

The CIR facility provides the capability to accurately control the ambient environment inside the chamber. This capability is provided by the Fuel and Oxidizer Mixing Apparatus (FOMA). The FOMA consists of gas bottles, pressure transducers and mass flow controllers connected to the combustion chamber. The contents of the chamber can be evacuated by a vacuum pump connected to the ISS overboard vent.

The hardware for the FLEX experiments is the Multi-User Droplet Combustion Apparatus (MDCA, Figure 1). The MDCA facility (Robbins and Shinn, 2010) is based on the design of the Space Shuttle Droplet Combustion Experiment (Nayagam et al., 1998). The MDCA is capable of deploying both free and fiber-supported droplets in a quiescent microgravity environment. The hardware for the deployment is 250 μm outside diameter stainless-steel tubes with polished and fluted ends. The fluid is dispensed between the axially opposed needles and then slowly stretched to a distance slightly smaller than the distance where the fluid would become detached from one of the needles. This stretch of the droplet between the needles minimizes the post-deployment drift velocity and internal circulation in the liquid. Just before ignition the needles rapidly retract, ideally leaving a motionless droplet *floating* in the middle of the CIR combustion chamber.

Once the needles retract, the control computer energizes two hot-wire igniters located 180 degrees to each other and in the same plane as the deployment needle assembly. After a preset time, the control computer de-energizes the igniters and activates the linear motors to retract them away from the droplet. For fiber-supported tests, the procedure is exactly the same except that

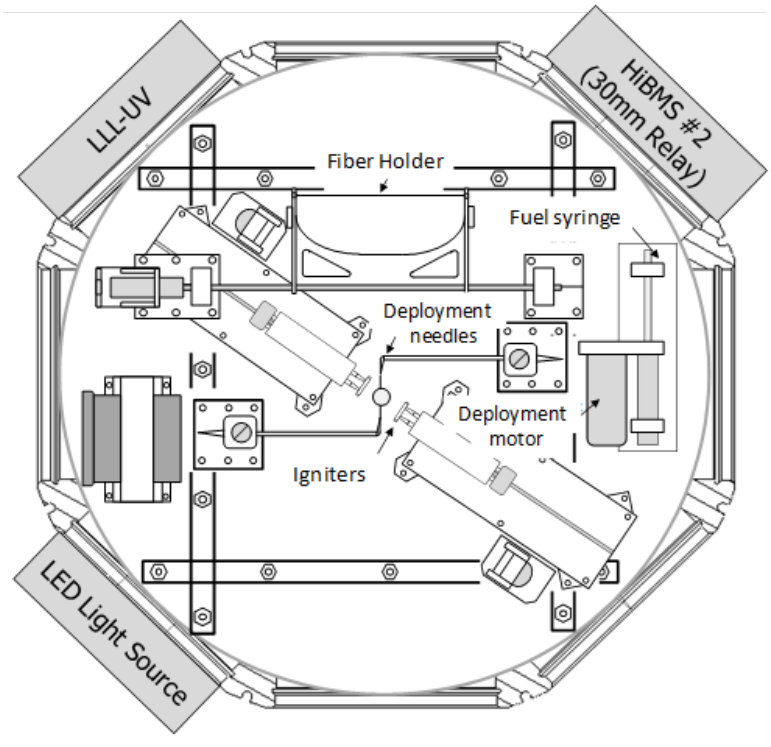

Figure 1: Schematic of the Multi-user Droplet Combustion Apparatus (MDCA). This is altered for clarity and is not the exact layout of the MDCA.

the droplets are deployed onto a small 80 μm Silicon-Carbide (SiC) support fiber.

Each needle is connected by flexible Teflon tubing to a fuel reservoir or cartridge. The fuel cartridges in the MDCA consist of a gas-tight syringe connected to a remotely actuated, gas-tight solenoid valve. The two reservoirs mounted in the MDCA are easily replaceable by the crew during nominal operations. For the experiments reported herein, each reservoir contained one of the test fuels. For the FLEX experiments the fuels were heptane and methanol. The on-going FLEX-2 experiments use octane and decane as well as several binary fuel mixtures and additional pure fuels. The FLEX-Italian Combustion Experiment for Green Air (FLEX-ICE-GA) used binary fuel mixtures of heptane and ethanol and decane and hexanol.

2.3.2 Experiment Diagnostics

The primary diagnostics for the FLEX experiment are provided by the CIR facility and described in detail elsewhere (Banu, 2008). They include a backlit view of the droplet and an orthogonal view of the flame. The illumination for the backlit view is a red laser diode source and a collimating optical system. They provide monochromatic illumination with a center wavelength between 650 - 660 nm. The laser diode operates below the lasing threshold current and thus acts as a non-coherent illumination source. The image system for the backlit view is the High Bit-Depth Multispectral (HiBMs) Package. The HiBMs Package has a telecentric imaging optical system and a high resolution 12-bit output digital camera. The HiBMS package is modular and can be configured on the ground and on-orbit with different lenses, filters, image configurations, etc.

Nearly all of the tests reported herein used the full 1024 x 1024 array with a fixed field of view of approximately 30 mm on a side. The images used the full 12 bits, and the framing rate was

30 fps. The HiBMS package, when used in conjunction with the illumination package, provided the capability of measuring the droplet size as a function of time and the soot volume fraction for soot-producing flames.

The CIR also provides a Low Light Level Ultra-Violet (LLLUV) package to image the chemiluminescence from OH^* of the burning droplet. The LLLUV package has a 1024 x 1024 monochrome frame transfer CCD array with 12 bit digital imaging capability. The CCD array is directly coupled to an 18 mm Gen-II-UV Micro-channel Plate Intensifier to provide maximum response at short wavelengths. The LLUV package includes intensifier and gating control that allows varied exposure times depending on the expected brightness of the flames. The LLLUV also has a spectral bandpass filter to image the chemiluminescence at 310 nm (the filter has a 10 nm FWHM bandwidth). Ground control of the LLLUV enabled pre-test setting of the gain, pixel binning and gate to optimally image the flames surrounding the droplets. All of the tests reported herein used the 2 x 2 binned (512 x 512 array) with a fixed field of view approximately 50 mm on a side. The framing rate for the majority of the tests was 30 fps, with a smaller number at 15 fps to attempt to improve flame contrast for very dim flames. The intensifier gain did vary somewhat over the tests in this report.

The final image view of the burning droplet is from a color camera. This camera view is augmented with illumination from a white LED located on the MDCA inside the CIR chamber. This camera has a zoom lens that provides the operators with a close-up view of the needles and droplet during droplet formation and stretch (providing near real-time feedback to maximize the success rate of the experiment). Immediately prior to droplet deployment and ignition the camera zooms out and the white LED turns off to provide an overview of the combustion process. The FOV of this camera is approximately 93 mm x 70 mm. This view provides flame size, shape and color information. This view is downlinked to the ground during nominal test point operations.

The entire CIR rack was mounted to the ISS through the Passive Rack Isolation System (PaRIS). The PaRIS isolated the CIR from any high frequency vibration or g-jitter that would disturb the experiment. The rack also had several Space Acceleration Measurement System (SAMS) heads mounted to it to monitor the acceleration level during the experiments. Examination of the SAMS data showed that the g-levels (across the frequency spectrum) were typically less than $10^{-5}g_0$ where g_0 is the acceleration due to gravity at sea level on earth.

2.3.3 Data Analysis

The data from the CIR cameras are stored digitally on the ISS until downlinked to the ground (typically within the same week of operation). The digital data, after de-compression, comes in the form of individual image files along with a file that contains the relevant timing information for all of the images.

Figure 2 shows a sequence of images for a burning heptane droplet from all of the CIR cameras, the left column being from the backlit image of the droplet, the center column from the LLUV, and the right from the color camera. The first row shows the droplet before deployment and the second row shows the powered ignitor coils (note the glow) prior to withdraw. Rows 3 and 4 in Figure 2 show the droplet and flame midway through the burn and just before flame extinction, respectively. The other rows show the droplet and flame images after visible flame extinction, the meaning of which will be clear later.

The backlight in the droplet images makes the discrimination between the droplet and background relatively easy (except when excessive soot formation obstructs the visibility of the droplet boundary (Dembia et al., 2012)). After defining a suitable threshold level, the droplet diameter is the size that results from equating the measured area of the droplet to that of an equivalent

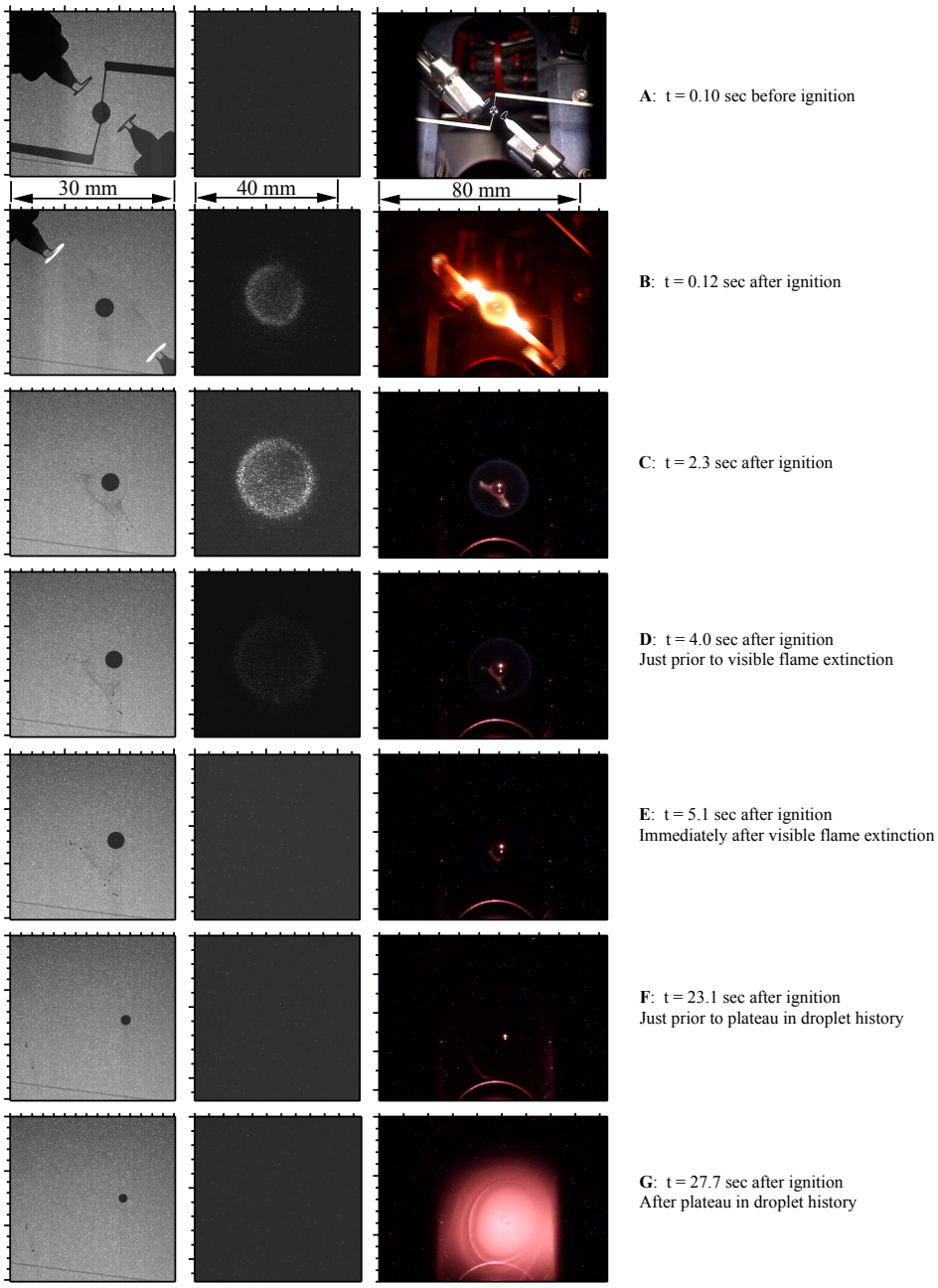

Figure 2: FLEX image sequence for a heptane droplet from the three cameras corresponding to the times denoted by the dashed lines in the subsequent figure. The left column is from the HiBMS camera, the center column from the LLUV camera and the right column from the color camera. The ambient oxygen and nitrogen mole fractions were 0.18 and 0.72, respectively and the ambient pressure was 1.0 atm.

circle (Struk et al., 1998). The average burning rate constant ($\bar{k}$) comes from a linear fit of the droplet-squared history between approximately $t = 0.1\tau_b$ and $0.9\tau_b$, where τ_b is the total burn time (igniter withdraw to extinction or burnout).

The flame size (both from the LLUV and color camera) is much more difficult to measure than the droplet size. Many of the flames were near the detectable limit in both cameras, and as a result quite dim. The flame luminosity also changed throughout the test, typically being brighter early in the burn and very dim near flame extinction. Using a single threshold value to discriminate between the flame and the background was problematic. A value relevant near flame extinction overestimates the flame diameter earlier, and a value relevant early in the flame lifetime does not detect a dim flame near extinction. For most of the tests reported herein the flame diameter is that which results from equating the measured area of the flame to that of an equivalent circle. The computer determined the threshold level to discriminate the flame from the background automatically using an iterative selection method (Ridler and Calvard, 1978). We found that this provided the best representation of the flame throughout the lifetime and represented the outer edge of the flame. For tests in which the flame area was too difficult to determine, the flame diameter was simply taken as the maximum dimension of the flame in the direction that exhibited the least noise throughout the test.

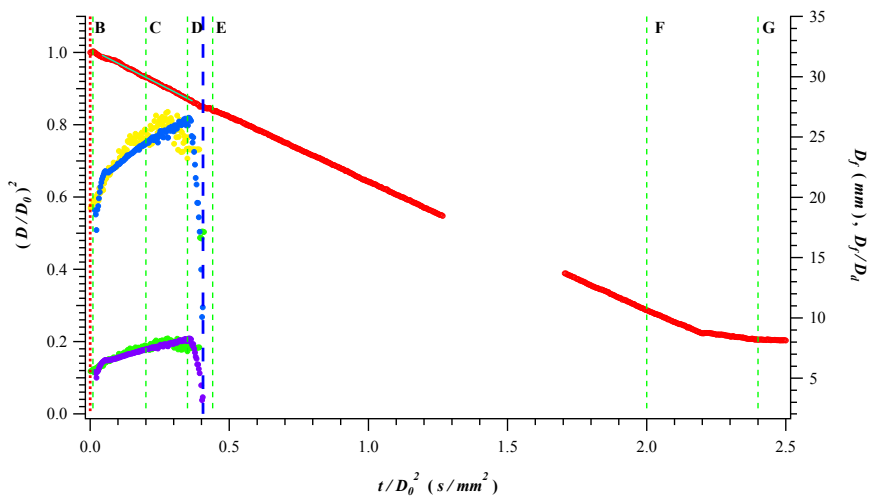

Figure 3: Droplet and flame histories for the heptane droplet in Fig. 2, initially 3.41 mm in diameter. The ambient environment had oxygen and nitrogen mole fractions of 0.18 and 0.72, respectively and a pressure of 1.0 atm. The gap in the droplet history at $t/D_0^2 \sim 1.5$ is when the droplet drifted out of the field of view of the HiBMS camera (the drift velocity was on the order of 1 - 2 mm/s). The thin vertical lines with letters correspond to the different times of the image sequence in Fig. 2. The thick dashed vertical line (coincident to when the flame diameter and standoff decrease quickly) is when visible flame extinction occurred.

Figure 3 contains the results of the analysis of the droplet and flame histories for the test in Figure 2. The plot shows the droplet diameter squared normalized by the initial diameter squared, flame diameter (upper curves) and flame standoff ratio (FSR),that is, the flame diameter normalized by the droplet diameter at the same time, all three variables as functions of the time normalized by the initial droplet diameter squared. The graph shows the flame size results for both the LLUV and color camera. The vertical line in Figure 3, where the flame size decreases rapidly, indicates when visible flame extinction occurs. The value of $\bar{k}$ is approximately 0.38 mm^s/s in this test.

After visible flame extinction the droplet drifts out of the field of view for a short period of time and then drifts back into the field of view. The reason why Figure 3 shows the droplet history beyond the visible flame extinction will be discussed in the following section.

2.3.4 Cool Flame Burning Mode

The early FLEX experiments showed that following the radiative extinction of large heptane droplets, the vaporization rate (slope of droplet diameter squared versus time) remained essentially constant for a long period of time (between E and F in Figure 3) after which the slope abruptly decreased (time G in Figure 3); this decrease corresponding to the appearance of a large vapor cloud in the color camera (the bottom row in Figure 2). This behavior is very different than that for smaller heptane droplets. Figure 4 shows two tests in the same ambient environment (air at 1.0 atm diluted with 5% CO_2). The plot in this instance is of the dimensional droplet diameter squared, flame diameter and FSR as functions of time.

The smaller droplet was slightly larger than 2 mm and the larger droplet slightly larger than 3 mm. The burning behavior was very different for the two droplets. The smaller droplet had an initially luminous yellow flame that quickly became a relatively bright blue. The flame size increased, reached a maximum midway through the burn and then decreased until the droplet disrupted at a very small size. Even though the flame size decreased through much of the flame lifetime, the flame standoff ratio (FSR) increased continuously for the most of the test before falling off rapidly just before extinction (the smaller droplet drifts out of the HiBMS field of view before extinction). The $\bar{k}$ for this test was approximately 0.53 mm^2/s.

The larger droplet had a slightly smaller $\bar{k}$ (0.49 mm^2/s) but very different flame behavior. The flame size grew continuously throughout the visible flame lifetime. In addition, after the initial ignition transient (where the flame is very luminous), the flame became very dim blue and the luminosity decreased continuously until flame extinction. The FSR increased continuously throughout the test although the rate of increase for the larger droplet was smaller. The total duration of the visible flame for the two droplets was nearly the same.

The linear vaporization behavior in this 'cool flame' region occurs as a result of low-temperature chemical reactions that somehow are initiated by the visible hot-flame extinction (Nayagam et al., 2012). Examining Figure 4 in more detail shows that the droplet diameter during this cool-flame regime is in the same range as that during the smaller droplet test. This means that for a given size range a droplet can burn with either a hot flame or a cool flame, the initial condition determining which mode the droplet burns in. A defining feature of this 'cool flame' mode is that it only occurs after radiative extinction of the hot flame. Its occurrence is also marked by vapor-cloud formation after cool-flame extinction. The heat release during this second-stage burning is approximately half of what is normally associated with n-heptane combustion and the activation energy associated with the chemical processes is similar to that of low-temperature ignition chemistry Nayagam et al. (2012).

Motivated by the FLEX experimental results, Farouk and Dryer (2014) carried out an exhaustive numerical study of n-heptane droplets burning in O_2/N_2, O_2/CO_2, and O_2/He environments. Figure 5 shows a comparison of a heptane burn that exhibited a cool flame with a numerical simulation (Farouk and Dryer, 2014). They used the n-heptane chemical kinetic model developed by Curran et al. (1998) consisting of 1038 species and 2739 reactions reduced using path flux analysis method to a manageable 128 species and 565 elementary reaction steps. The inclusion of low temperature chemistry[1] enabled them to qualitatively predict the second-stage burning of

[1]Earlier modeling efforts used only high temperature kinetics, since this permitted a significant reduction in computational time as there was no experimental evidence or suspicion of low temperature kinetic significance.

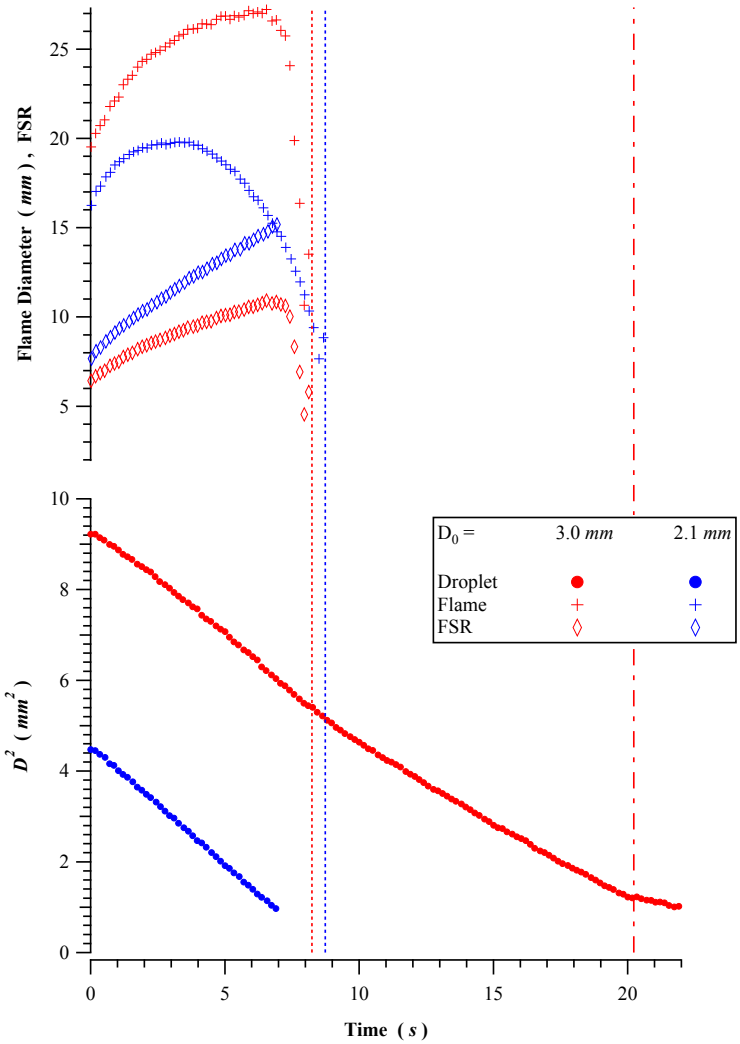

Figure 4: Droplet and flame histories for two heptane droplets (D_0 = 2.1, 3.0 mm) burning in a 0.20/0.75/0.05 $O_2/N_2/CO_2$, 1.0 atm ambient environment. The flame is that measured by the LLUV. The smaller droplet drifted out of the field of view before the end of the test. The vertical dashed lines indicate the time where flame extinction occurred; the dashed line at 20+ s marks the approximate time of the second extinction. For clarity, the graphs show a subset (one of every five) of the experimental data.

n-heptane droplet in air at atmospheric pressure shown in Figures 3 and 4.

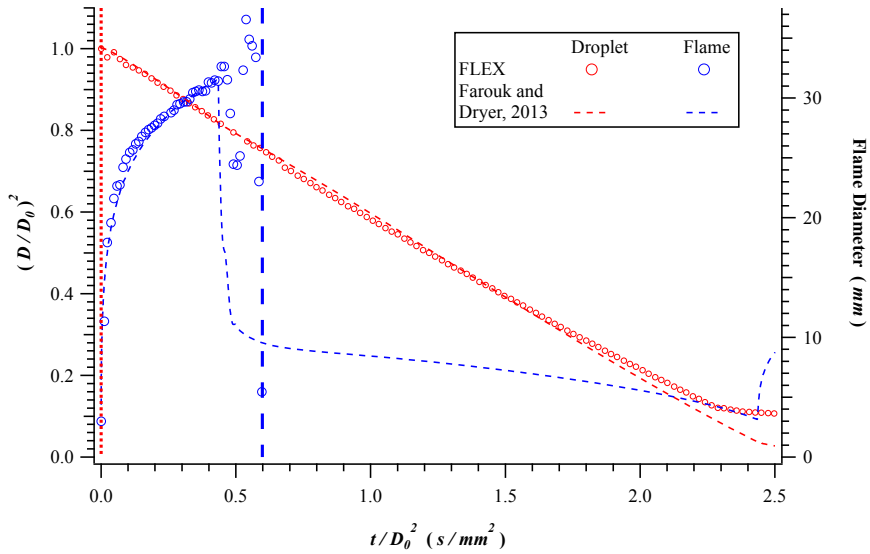

Figure 5: Experimental (FLEX) and predicted (Farouk and Dryer, 2014) droplet and flame histories for a heptane droplet ($D_0 = 3.9mm$) burning in a nominally air (0.21 oxygen mole fraction, balance nitrogen), 1.0 atm ambient environment. The numerical predictions contain both high and low temperature chemistry. For clarity, the graphs show a subset (one of every ten for the droplet, one of every five for the flame) of the experimental data.

Figure 5 shows that the detailed model with the kinetic mechanism developed from Curran et al. (1998) over-predicted the second-stage burning rate and under-predicted the droplet extinction diameter by almost a factor of 3.5. Farouk and Dryer (2014) identified two low temperature reactions that had the most influence on the second stage burning, isomerization of $QOOHO_2$ to ketohydroperoxide ($QOOH_2 \rightarrow Ketohydroperoxide + OH$) and dissociation of $QOOHO_2$ ($QOOHO_2 \rightarrow QOOH + O_2$). When the reaction rates of the first reaction was decreased by a factor of 2 and the second reaction increased by a factor of two the agreement between the predictions and the experiments improved. They also point out the need for further improvements in terms of mechanistic structure and rate uncertainties for the low temperature reactions, as is also evidenced in other alkane oxidation studies by Dryer's group (Jahangirian et al., 2012). The study further shows that the same modifications that improve the agreement with the FLEX experiment results also lead to improved predictions with published ignition delay times and oxidation speciation for n-heptane.

The numerical predictions utilize a detailed chemical kinetics model containing both high and low temperature chemistry in a spherically-symmetric droplet combustion model. The predictions from the model for the droplet history capture the two stage combustion behavior; the visible extinction of the flame, transition to the second stage and self sustaining continuous combustion in the second stage. The numerical predictions show the peak gas temperature during the second stage to be approximately 700 K denoting the presence of low temperature chemistry. The numerical predictions (Farouk and Dryer, 2014) identify the radiative heat loss as being responsible for initiating the 'cool flame', consistent with the experimental observation (Nayagam et al., 2012).

Ambient hot wire ignition led to high temperature burning, essentially to extinction. The high temperature kinetic model of Chaos et al. (2007) eliminated consideration of low temperature behavior such that the second-stage low temperature burning effects were never considered.

The model also predicts the presence of gaseous pure fuel vapor in addition to larger alkenes, ketohydroperoxides and cyclic ethers after 'cool flame' extinction that could condense to form the vapor cloud observed in the experiments.

Prior to the FLEX results, Cuoci et al. (2005) simulated microgravity vaporization, autoignition and combustion of n-heptane and n-decane droplets using the detailed chemical kinetic scheme of Ranzi et al. (1995) with approximately 200 species and more than 5000 reactions and including gas-phase radiative heat loss. They were able to successfully predict multi-stage ignition and radiative flame extinction. They did not, however, report the cool flame supported quasi-steady burning observed in the FLEX experiments. This is likely because the authors limited their large droplet simulations to n-heptane droplets burning in oxygen-helium mixtures at atmospheric pressure for which experimental measurements were available (Nayagam et al., 1998; Choi and Dryer, 2001). Recent analyses of these experiments by Farouk and Dryer (2014) predicted that two stage burning behavior may have been present, but that the second stage characteristic burning time was too short to be resolved in the analysis of the experimental data. More recently, Cuoci et al. (2013) updated their analysis and compared their numerical predictions with second-stage burning results of Nayagam et al. (2012) and arrived at similar conclusions.

2.4 Summary of FLEX Cool Flame Experiments to Date

The original objectives of the FLEX experiments were to examine flammability limits of isolated pure fuel droplets (heptane and methanol) and inert gas fire suppressant efficacy. The follow-on FLEX-2 investigation was more fundamental investigating the burning of single droplets of a range of fuels, fuel mixtures and even binary arrays of droplets. The focus in both experiments was on the hot flame burning and extinction; the cool flame regime a serendipitous discovery. The experimental data in Figures 3, 4 and 5 represent ideal tests, free droplets that exhibited minimal drift and stayed in the imaging systems fields of view, prolonged cool flame burning and an identifiable cool flame extinction.

These tests represent a subset of the total tests where cool flame burning was observed or known to occur. Observation of the complete burning history of a droplet during both the hot and cool flame regimes requires it to remain in a very small field of view (30 mm x 30 mm) for, in some cases, over 60 seconds. Since the droplet is deployed in the center of the field of view, this means combined residual velocities (due to deployment, ignition, and g-jitter) of 0.25 mm/s or less. Fiber support provides a means of fixing the droplet in space. The support fiber for the FLEX experiments is an 80 μm silicon-carbide (SiC) fiber, selected for its strength and durability. The FLEX experiments show that the fiber can 'fix' the droplet in space and capture the hot flame (even providing an estimate of the hot-flame temperature with one of the CIR cameras), hot flame extinction and quasi-steady cool flame burning. Near cool flame extinction, however, the fiber-supported experiments show significant droplet oscillations and disruptions on the fiber making the accurate determination of the cool flame extinction diameter almost impossible.

The original FLEX experiments had diagnostics that were selected and optimized to view the hot flame and hot flame extinction. The cool flames are much lower in temperature, have different spectral emission characteristics and much lower heat release rates than the corresponding hot flames. As a result, the cool flames are essentially invisible to the CIR imaging systems on FLEX. The radiometer package originally installed on the MDCA did not function properly (unacceptably low signal to noise ratio) and was replaced for FLEX and FLEX-2 experiments starting in 2012. The new radiometer package consisted of a wideband radiometer that is sensitive over the visible into the far infrared and a narrowband radiometer that is filtered around a strong water vapor emission band centered at approximately 6 μm. The new radiometer package had much better

signal to noise characteristics with the fixed gain on the wideband optimized to be sensitive to the hot flame and the fixed gain on the narrowband optimized to be sensitive to the cool flame.

The FLEX experiments burning heptane showed that cool flames can occur in a wide range of experimental conditions. The experiments to date show the cool flame requires radiative extinction of a hot flame to exist. Between the start of the FLEX tests in 2009 and the end of 2011 there were approximately 53 heptane tests where the flame radiatively extinguished. These experiments had the original MDCA radiometers and thus it is difficult to know in some cases whether there was a cool flame stage; its presence implied by the linear d-squared regression and the vapor cloud.

In January 2012 FLEX-2 testing started. This included (with tests on-going) tests with pure normal octane, decane and propylbenzene and mixtures (50/50 by weight) of decane and propylbenzene as well as continued tests with pure heptane. More recently, NASA collaborated with the Italian Space Agency and Istituto Motori, C.N.R. - Naples on the FLEX Italian Combustion Experiment for Green Air (FLEX-ICE-GA). The tests for this series of experiments involved mixtures (50/50 by weight) of heptane and ethanol and also decane and hexanol. Cool flames existed for many of the fuels and ambient conditions during the FLEX-2 and FLEX-ICE-GA tests, the results of which will be summarized in the subsequent subsections.

Nearly coincident with the start of the FLEX-2 tests was the installation of the new radiometer package. The new radiometers, particularly the narrowband radiometer, were sensitive to the cool flame and could detect both the cool flame burning and, most importantly, the cool flame extinction. Through calibration with a blackbody source on the ground and then subtraction of the igniter radiance, the radiometers provide a measure of the the total flame radiance (wideband) and total flame radiance at approximately 6 μm (narrowband).

Figure 6 shows the results of a particularly good test with heptane burning in a nominally air ambient. After ignition, the initially 3.6 mm droplet burns with a hot flame that extinguishes at a diameter of 2.84 mm. The wideband radiometer tracks the hot flame diameter very closely during this period with a peak flame radiance of approximately 20 W. During the hot flame and early in the cool flame, the narrowband radiometer saturates (fixed gain) and is not displayed in Figure 6. The hot flame is followed by a long period of cool flame burning. At a normalized time of approximately 2.2 s/mm^2 the narrowband radiometer shows a distinct inflection point where the slope of flame radiance with time abruptly decreases. This point is coincident with the beginning of the plateau in the droplet history and the formation of the vapor cloud and is thus in all likelihood the extinction of the cool flame. The total flame radiance during the cool flame is more than an order of magnitude smaller than the flame radiance during the hot flame.

The following subsections highlight some of the major observations from the FLEX, FLEX-2 and FLEX-ICE-GA tests.

2.4.1 Cool flames are prevalent

The cool flame phenomena is not limited to a single fuel or narrow range of ambient conditions. They occur with all of the normal alkane fuels over a wide range of pressure, ambient oxygen mole fraction and ambient gas composition. They occur almost exclusively as a result of radiative extinction of the hot flame. There are a few tests where after the igniters withdraw there is not hot flame. These tests are likely ones in which the heat release from combustion and delivered ignition energy were only sufficient to produce the low temperature kinetic activity driving the combustion into the negative temperature coefficient kinetic regime, but not through hot ignition. Outside of these few tests, however, cool flames only occur after radiative extinction of the hot flame. Moreover, the period of cool flame burning is influenced by the initial experimental conditions and drop size, sometimes producing such short characteristic burning times as to clearly identify cool

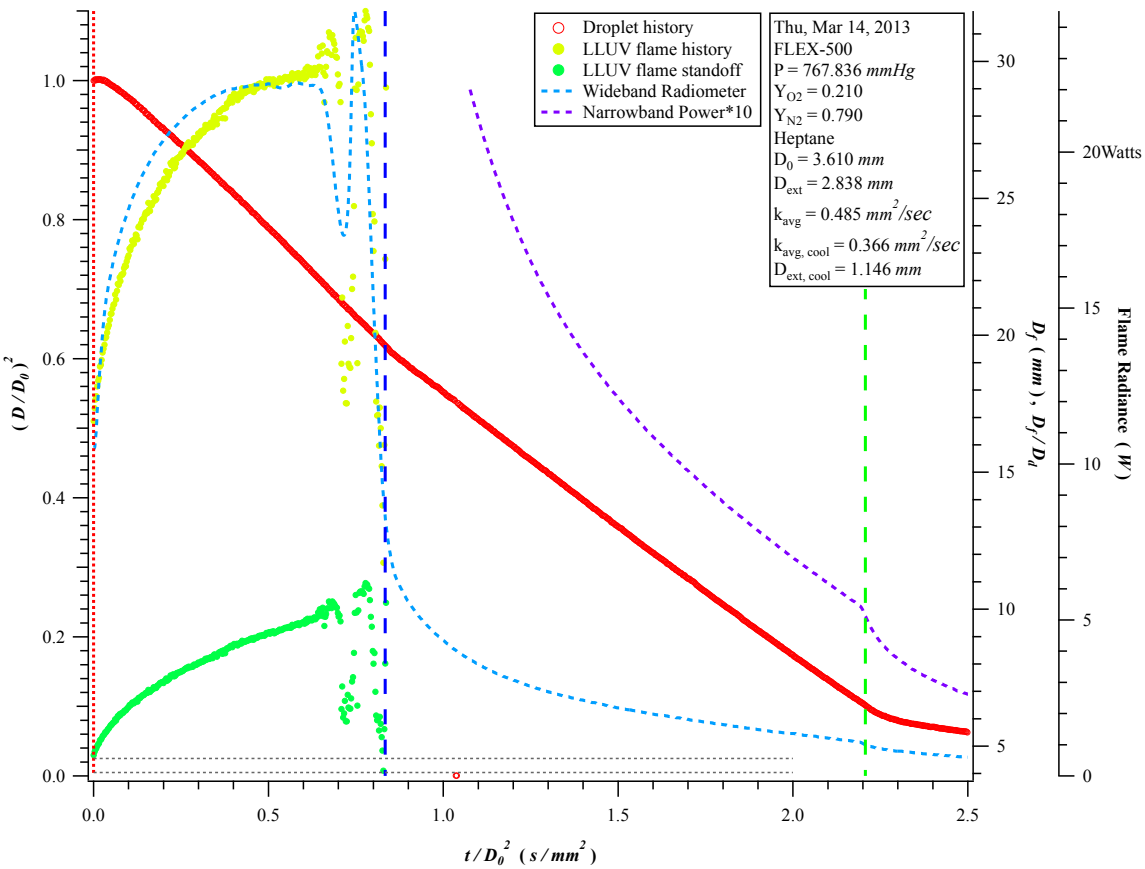

Figure 6: The droplet, flame and radiometer histories for a heptane droplet ($D_0 = 3.61mm$) burning in a nominally air (0.21 oxygen mole fraction, balance nitrogen), 1.0 atm ambient environment. The droplet diameter and time are both normalized by the initial droplet diameter squared. The narrowband flame radiance is scaled by a factor of 10 to put it on the same scale as the wideband flame radiance.

flame behavior.

The prevalence of cool flames raises the question as to why their presence had not been observed in previous microgravity experiments. Schnaubelt et al. (2000) and Tanabe et al. (1995) did observe a cool flame briefly during ignition experiments with heptane. Cuoci et al. (2005) predicted the occurrence of a cool flame during heptane auto-ignition and further asserted that the presence of cool flames explained the unique experimental observations of Xu et al. (2003). Despite the intense work in microgravity droplet combustion by NASA, ESA and JAXA, however, cool flames were not observed or predicted after hot flame extinction.

Much of this is due to limitations in the available test time. The FLEX experiments show that the quasi-steady cool flame occurs primarily after radiative extinction of the hot flame, especially under the application of strong ignition energy conditions.. To achieve radiative extinction requires test times greater than that typically available in drop towers[2] primarily because droplets of sufficient diameter to achieve radiative extinction cannot be produced in the available test time.. Dietrich et al. (2005) performed experiments with decane in the Japan Microgravity Center 10 second drop tower. The experiments involved radiative extinction in ambient conditions where cool flames were likely. The cameras, however, lacked the low light sensitivity to see the cool flame and the duration of cool flame burning before the test concluded (impact at the bottom of the drop tower) precluded observing the prolonged linear regression of droplet diameter squared and the formation of the vapor cloud.

The NASA Droplet Combustion Experiment (DCE, Nayagam et al., 1998) studied heptane droplet combustion in helium-diluted ambient environments. The test matrix included, based on the current FLEX experiments, conditions where radiative extinction occurred and also support cool flames. Again, however, the camera systems, selected to visualize the hot flame, lacked the low-light sensitivity to image the cool flame. Further, Farouk and Dryer (2014) recently showed that cool flames likely existed but the predicted cool flame extinction droplet diameters were very close to the experimentally-measured hot flame extinction diameters. This means the time of cool flame burning was very short and again there was insufficient time to observe the linear regression of droplet diameter squared with time and the vapor cloud, if it formed at all, would have been unremarkable.

The NASA Fiber Supported Droplet Combustion (FSDC, Dietrich et al., 1996) and FSDC-2 experiments included studies of alkane fuels in nominally air, one *atm* pressure ambient environments. These small-scale experiments glovebox experiments used facility-provided video cameras that lacked the low-light sensitivity to observe even the dim hot flames. In retrospect the reported observations of these experiments (Dietrich et al., 1996; Shaw et al., 2001) suggest that cool flames were indeed present, but the limited diagnostics made definitive conclusions regarding their existence problematic.

2.4.2 Significant effect of ambient pressure

The ambient pressure has a large influence on both cool flame formation and cool flame extinction. Without any diagnostics to detect cool flames, the early FLEX tests used the unusual observation of linear d-squared behavior after hot flame extinction and vapor cloud formation as the indicators of cool flame burning. The early FLEX tests showed that at sub-atmospheric pressure ambients it was almost impossible to infer the existence of the cool flames with heptane from the experimental data (using the original radiometer package). This means that there was a very short or no linear

[2]While aircraft flying parabolic trajectories have test times where cool flames could be observed, the gravitation levels create buoyant flows that destroy the spherical symmetry and make radiative extinction almost impossible to observe (e.g., Struk et al., 1997).

portion of the d-squared history after hot flame extinction and no (or very small) vapor cloud formation. Evidently the cool flame burning, if it existed at all, was for a very short time.

This is somewhat borne out by examining the decane data which included sub-atmospheric tests and had the new radiometer package available. Figure 7 shows two decane droplets (both freely deployed) at 1.0 and 0.5 *atm*. The ambient oxygen mole fraction was 0.21 (balance nitrogen) for both tests. The initial droplet sizes for the two tests were very close. Figure 7 clearly shows that the hot flame behavior for both tests was nearly identical; the droplet histories (normalized by the initial diameter squared) overlapping and hot flame extinction occurring at nearly the same normalized time. After hot flame extinction, however, the cool flame behavior is significantly different. The cool flame burning rate for the 1.0 *atm* test is much higher and the cool flame extinction droplet diameter much smaller. Examination of the wideband radiometer shows a hot flame radiance the is very similar for both tests, but the cool flame radiance for the 1 atm test is much larger than that of the 0.50 *atm* test. The narrowband radiometer data shows that the cool flame extinguishes at nearly the same value of the flame radiance, but that radiance occurs at a much smaller droplet diameter for the 1.0 *atm* test.

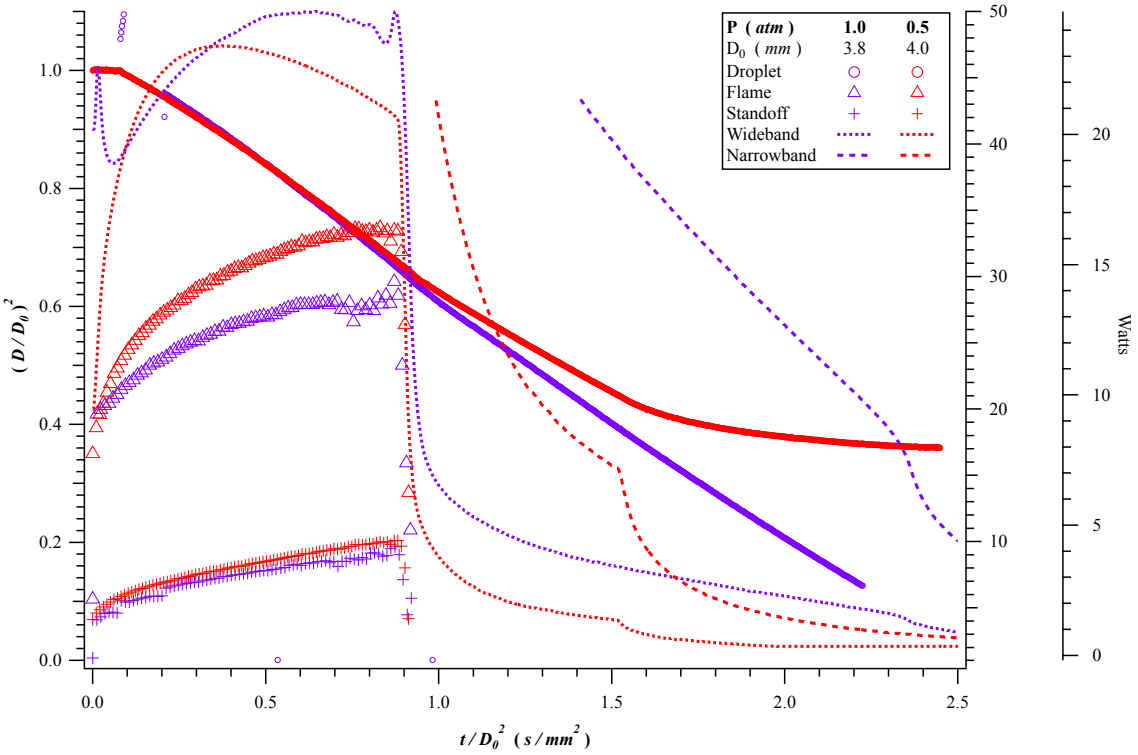

Figure 7: The droplet, flame and radiometer histories for two decane droplets burning in a 0.21 ambient oxygen mole fraction (balance nitrogen) environment and 0.50 and 1.0 *atm* pressure. The droplet diameter and time are both normalized by the initial droplet diameter squared. The narrowband flame radiance is scaled by a factor of 10 to put it on the same scale as the wideband flame radiance.

The hyperbaric behavior of the cool flames is significant as well (Farouk et al., 2014). Figure 8 shows the result of a fiber-supported (free deployment was problematic at the high pressure conditions) heptane droplet burning in a 3.0 *atm* ambient environment. Unlike in the atmospheric and sub-atmospheric pressure tests, the hot flame extinction extinction is not discernible in the

wideband radiometer. It was, however, evident from the $OH*$ chemiluminescence and the glow of the SiC fiber. The burning rate during the hot flame is quite high, approaching 0.9 mm^2/s and remains high during the cool flame burning following hot flame extinction. There is significant noise in the droplet history that is a result of the significant droplet motion and mini-disruptions on the fiber (that complicates the droplet size measurement). Some time after hot flame extinction the cool flame briefly re-ignites the hot flame as evident in the wideband radiometer trace on the graph as well as in the flame images. The flame radiance during this reignation is much higher than the flame radiance during the hot flame, actually saturating the wideband radiometer. This suggests that the reignited hot flame is either a pre-mixed or partially pre-mixed flame propagating through the fuel vapor/air mixture that results from the unconsumed fuel during the cool flame period mixing with ambient air. The narrowband radiometer, so useful in identifying cool flame extinction in the atmospheric and sub-atmospheric pressure tests, is saturated until well after the droplet disappears and the test is complete. Farouk et al. (2014) demonstrated the the ability to predict the qualitative re-ignition behavior in addition to quantitatively predicting many of the experimental observations.

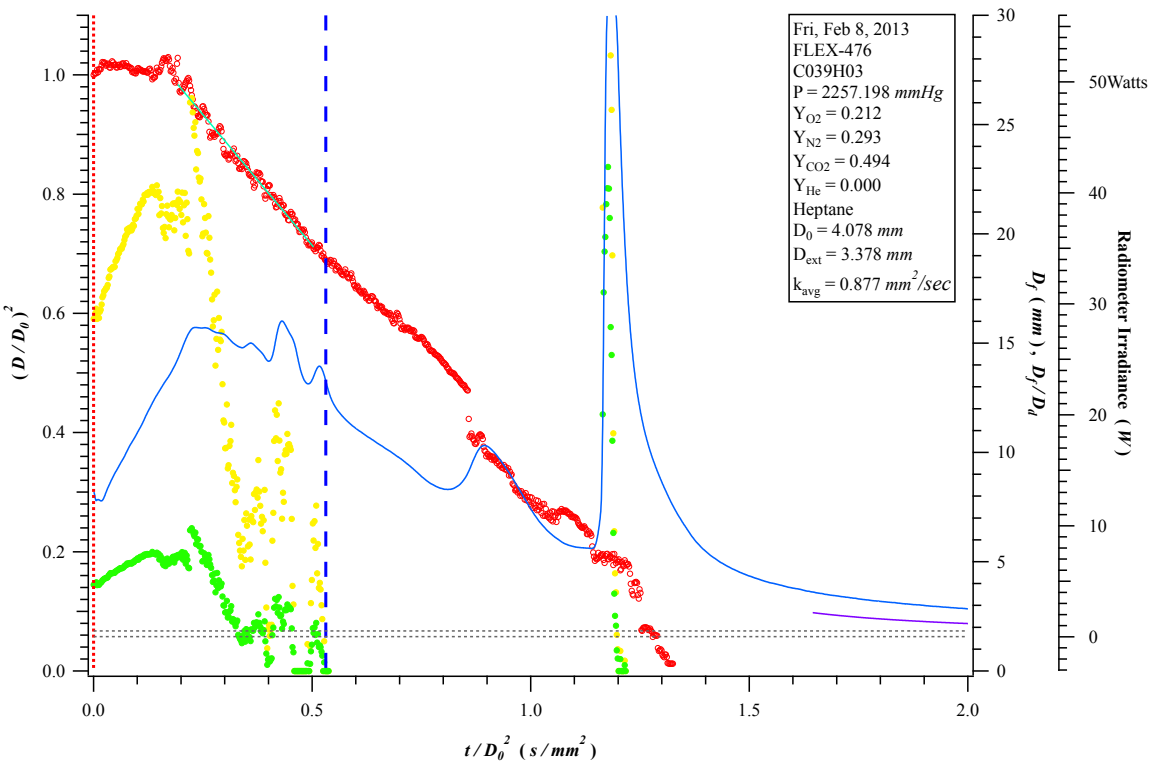

Figure 8: The droplet, flame and radiometer histories for a heptane droplets burning in a 0.21 ambient oxygen mole fraction (0.30 nitrogen and 0.50 carbon dioxide) environment and 3.0 atm pressure. The droplet diameter and time are both normalized by the initial droplet diameter squared.

2.4.3 The effect of ambient gas composition

One of the original objectives of the FLEX experiments was to provide fundamental information on the efficacy of inert gas fire suppressants. By leveraging the spherical symmetric combustion of

isolated liquid fuel droplets, the experiments sought to systematically vary the inert gas concentration in nominally air (0.21/0.79 oxygen/nitrogen mole fraction, 1.0 atm) and pre-EVA (0.30/0.70 oxygen/nitrogen, 0.70 atm) ambient environments for a range of inert gases including nitrogen, carbon dioxide, helium and xenon, and determine the flammability limits. The tests involved varying the initial diameter to examine both the diffusive extinction (or burnout) and radiative extinction limits in ambients with increasing inert gas concentrations. Cool flames occurred in almost all ambient environments after radiative extinction of the hot flame. The cool flame burning behavior, however, was a strong function of both the ambient oxygen mole fraction and diluent gas.

Figure 9 shows how replacing some of the nitrogen with helium influenced both the hot flame and cool flame burning for n-octane droplets. The two droplets in the plot burned in 1.0 atm, 0.21 oxygen mole fraction ambient environments where some of the nitrogen gets replaced with helium. The helium mole fractions (balance nitrogen) for the two tests were 0.15 and 0.50. Increasing the helium concentration influences both the hot and cool flame burning behavior. The average burning rate constant for both the hot and cool flame regimes was higher for test with the higher helium ambient mole fraction. The hot flame extinguished quickly for the higher ambient helium mole fraction test and the cool flame burning period was also short with the cool flame extinction droplet diameter larger than the hot flame extinction droplet diameter for the test with the smaller ambient helium mole fraction. Interestingly, while the test in the higher ambient helium mole fraction atmosphere had a higher burning rate constant, the flame radiance was actually lower.

2.4.4 The effect of fuel composition

The FLEX tests to date show that the cool flame burning regime is prevalent for the n-alkane fuels studied (heptane, n-octane and decane). The FLEX tests with methanol, as expected, did not show a cool flame burning regime. The FLEX-ICE-GA series of tests involved mixtures of heptane/ethanol and decane/hexanol (50/50 by weight for both). Figure 10 shows the result of a large heptane/ethanol droplet burning in a nominally air ambient (0.21/0.79 oxygen/nitrogen, 1.0 atm). Comparing this test to the pure heptane test in Figure 6 shows how fuel composition can influence the cool flame regime. The pure heptane droplet radiatively extinguishes and then has a prolonged period of cool flame burning with the cool flame extinguishing at a droplet diameter slightly larger than 1 mm. The cool flame burning is characterized by the linear d-squared behavior and the cool flame extinction by the formation of the fuel vapor cloud and the abrupt change in the slope of the narrowband radiometer. The heptane/ethanol mixture droplet, however, does not exhibit the linear d-squared behavior after visible flame extinction. Nor is there a vapor cloud or the abrupt change in the slope of the narrowband radiometer. All of this implies that the addition of ethanol to the heptane inhibits the cool flame burning. These results are consistent with experimental and modeling studies in flow reactors (Haas et al., 2009, 2011).

The decane/hexanol mixture droplets did exhibit cool flame behavior, including multiple re-ignitions of the hot flame at hyperbaric pressures.

2.5 Summary

The objectives of the FLEX, FLEX-2 and FLEX-ICE-GA experiments were to study various aspects of isolated fuel droplet hot-flame burning and extinction. In addition to providing insights into the combustion of liquid fuel droplets, they were very successful in identifying the cool flame burning regime; something originally thought could not exist. The experiments showed that cool flame burning is prevalent and that ambient pressure, oxygen mole fraction, diluent gas and composition and fuel composition strongly influence the cool flame burning behavior. These experiments,

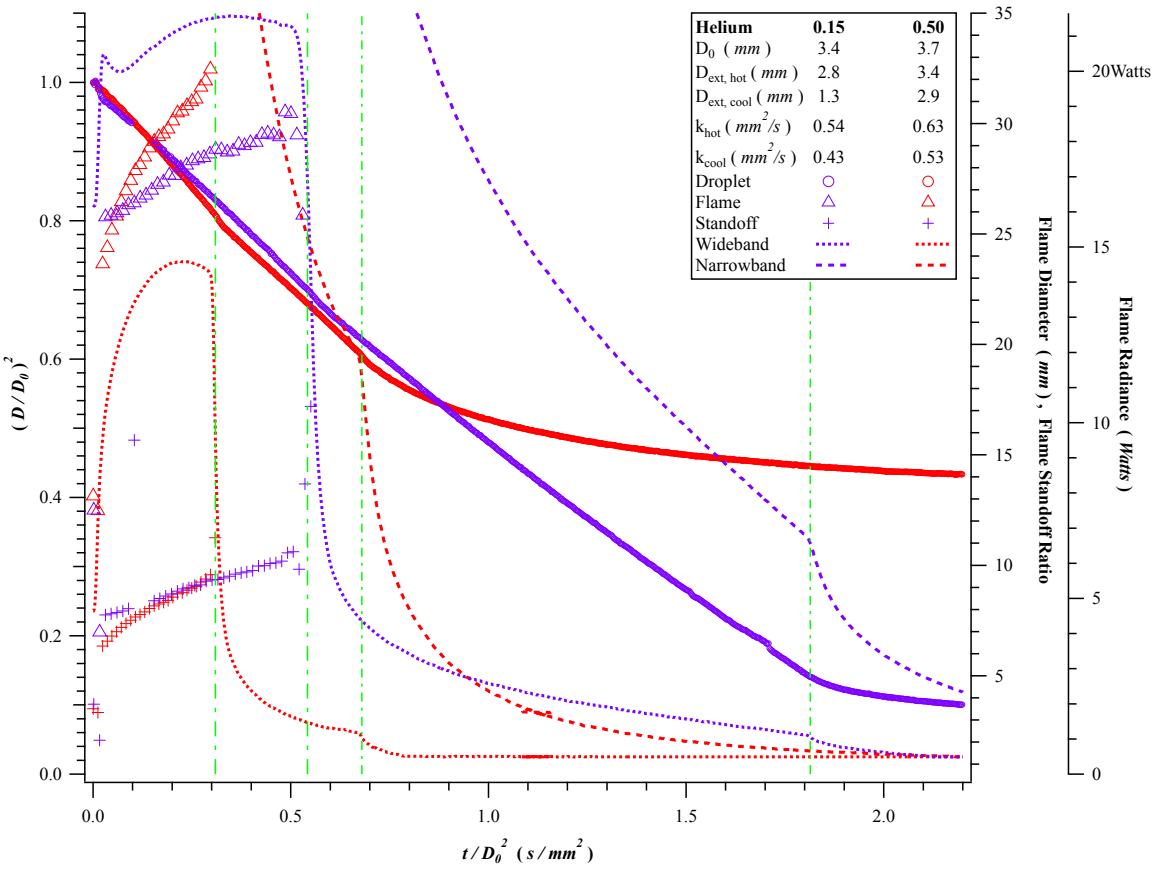

Figure 9: The droplet, flame and radiometer histories for n-octane droplets burning in a 0.21 ambient oxygen mole fraction at 1.0 *atm* pressure. The diluent gases in the two tests were nitrogen/helium mixtures with helium mole fractions (balance nitrogen) of 0.15 and 0.50. The narrowband radiometer is scaled by a factor of 10 so it can appear on the same scale as the wideband data.

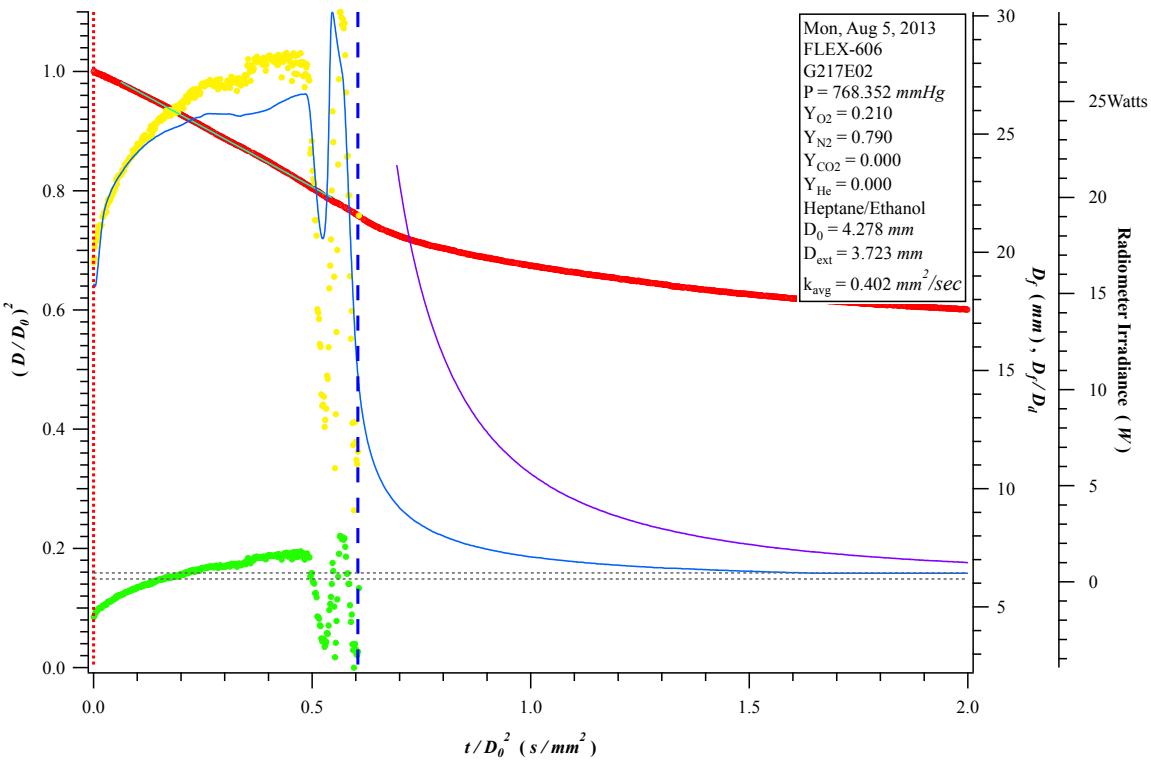

Figure 10: The droplet, flame and radiometer histories for heptane/ethanol droplet burning in a nominally air 0.21/0.79 oxygen/nitrogen, 1.0 atm) ambient environment. The narrowband radiometer is scaled by a factor of 10 so it can appear on the same scale as the wideband data.

however, were not intended and the test matrix not designed for the purposes of explicitly studying low temperature chemistry. The diagnostics were designed and optimized to be sensitive to the hot flames and, with the notable exception, of the new radiometer package, were not sensitive to the cool flame. As a result, there is no experimental data regarding the structure of the cool flame or its behavior as a function of time.

The experiments proposed in the next section seek to improve our understanding of low temperature chemistry by leveraging the spherically symmetric geometry of isolated fuel droplets burning in microgravity. The new experiments will study fuels, fuel mixtures and additives that will both promote and inhibit cool flame burning. The new experiments will be augmented with diagnostics that will provide information regarding the structure and temporal behavior of the cool flames.

3 Experiment Objectives

As described in the previous section, cool flame phenomena are influenced by a number of factors, including the fuel molecular structure (for pure fuel cases), the ambient environment (pressure, temperature, oxygen and diluent concentrations), and the fuel composition (the mixture of fuel structures and perhaps fuel additives such as those used to change octane or cetane behavior).

The overall goal of the proposed experiments is to improve our understanding of low temperature chemistry by studying the cool flame burning and, most importantly, cool flame extinction of droplet burning with spherical symmetry in a long-duration microgravity environment. The experiments to date show that prolonged cool flame burning (in some cases up to 60 seconds) is possible. The quasi-steady cool flame burning regime abruptly ends at cool flame extinction at a finite droplet size, something easily identified in the proposed experiments. By varying the fuels and ambient conditions, the experiments to date show that we can effectively, and over a wide range, vary the cool flame extinction diameter which allows for the varying the characteristic time scales of the cool flame chemistry. This in turn will provide experimental data that can be used to both validate and improve simplified and detailed low temperature chemical kinetic models.

3.1 Objectives of the proposed effort

The primary objectives of the proposed experiments are as follows:

1. *Further understanding of the combustion characteristics of normal alkanes, particularly in the low temperature region by conducting droplet combustion experiments in low gravity with fuels that supports cool flame burning and extinction.*

2. *Investigate the low temperature burning behavior of droplets consisting of pure fuels and bio-fuel constituents (and mixtures of them), as well as surrogate reference fuels to determine the relationship between the cool flame burning characteristics in microgravity droplet combustion and the octane/cetane behavior of the fuel.*

3. *Explore the low temperature chemistry of alkanes further by mixing additives to the fuel that disrupt the low temperature chemical pathways.*

3.2 Fuel

3.2.1 Baseline Fuel

The molecular composition of a fuel has a profound effect on the relative importance of low, negative temperature coefficient (NTC), intermediate, and high temperature kinetic behavior. The low temperature, NTC and hot ignition kinetic behavior and associated heat release are key features relating to premixed cool flames and microgravity droplet combustion cool flame behavior as well as engine knock and compression ignition phenomena. Ground based kinetic experiments with C7 through C16 n-alkanes show increasingly more low and NTC behavior up to about C12. FLEX experiments to date have also shown that cool flame behavior will occur with n-heptane, n-octane, and n-decane. And it is expected that n-dodecane will be even further active than these species.

Therefore in this study we propose to extend normal alkane experiments to include pure n-dodecane. The molecular weight of n-dodecane is near the average of that found for petroleum jet fuels and somewhat less than what is found for diesel fuels. The study of larger n-alkanes is not necessary as it was noted above that carbon chain length, the production of ketohydroperoxides and the resulting degenerate chain branching is no longer limited by the statistical probability

of O2QOOH isomerization through five and six membered ring formation. Though considerable ground based work has recently been produced on n-dodecane combustion kinetics, cool droplet burning research will add to improving our understanding of its low temperature and NTC behavior.

3.2.2 Isomeric Fuels and Surrogate Fuel Blends

Alkane isomeric structure can significantly reduce low temperature and negative temperature kinetic behavior of a pure alkane relative to an n-alkane of equal carbon number. The reduced activity is caused by reducing the probabilities of five and six member ring formation. For example, two recently produced renewable fuel components, farnesane (2,6,10 trimethyldodecane), and 2,2,4,6,6 pentamethylheptane of carbon number similar to n-dodecane have derived cetane numbers of 58 and 15 in comparison to n-dodecane and its derived cetane number of 78 (the higher the cetane number, the more active low temperature and NTC chemical behavior. We propose to study these two new alternate fuels in pure form to compare both their high temperature and cool droplet burning behavior in relationship to n-dodecane. Mixtures of n-dodecane with each of these renewable alternative fuels are also proposed to be studied, in order to understand the interactive influence of their chemistries on cool droplet burning behavior.

Finally, the blending of two or more molecular structures can also be used as a means of varying low temperature and NTC kinetic behavior. The Primary Reference Fuel (PRF) mixtures of n-heptane and 2,2,4 trimethylpentane (iso-octane) are used to emulate the behavior of real gasolines and define the Octane number of a gasoline. Another mixture used for this purpose are termed Toluene Reference Fuel (TRF) mixtures. We propose to study PRF and TRF mixtures that produce octane values of 50, 70, and 90.

Moreover, experiments on gas turbine fuels in drop towers and in other ground based facilities have been studying surrogate fuel mixtures of n-dodecane, iso-octane, n-propyl benzene, and 1,3,5 trimethyl benzene to emulate real gas turbine fuel behaviors, which also manifest cool flame kinetic phenomena. We propose to utilize one specific mixture that has been formulated and studied previously to emulate a global Jet A real fuel.

All of the above investigations contribute significant, new fundamental science that has strong potential for contributing to methodologies to controle the autoignition behavior of future petroleum derived and renewable derived fuels and their blends (Santana et al.).

3.2.3 Fuel Additive

Certain additives such as nitrates and peroxides when mixed with fuels alter their combustion chemistry and reaction pathways by disrupting the availability of radicals in the oxidation chain reactions. In some cases they are known to improve performance of diesel and other bio-fuel fired engines. In this study we choose di-tertiary-butyl-peroxide ($C_8H_{18}O_2$) as an additive to be blended with n-dodecane. Earlier studies in rapid compression machines has shown substantial reduction in ignition delay times when small amounts of DTBP is added to the fuel Tanaka et al. (2003).

3.3 Ambient Conditions

The ambient gas in the proposed study is a mixture of oxygen and nitrogen. The oxygen mole fraction will be varied in the range 0.18 to 0.35. The total pressure of the combustion chamber will be varied in the range 0.5 to 5.0 atm. The initial combustion chamber temperature will be maintained around 25^0 C and the relative humidity maintained at less than 10%.

Helium dilution studies will provide us with the ability to control cool flame extinction diameters over a larger range than simply using oxygen/nitrogen mixtures. The FLEX tests to date show

that large variations in cool flame extinction diameter can be affected by relatively small changes in the ambient helium concentration.

The FLEX experiments show that xenon dilution will lead to long cool flame burning and burning at lower ambient oxygen mole fractions than in with either nitrogen or helium dilution. This will greatly change the characteristic time and length scales and provide a wide parameter space with which to compare against theory/modeling.

4 Microgravity Justification

The objective of this experiment is to use the spherically-symmetric combustion of an isolated fuel droplet as a model geometry for cool flame formation and extinction. In order to completely leverage the droplet geometry, it is critically important to maintain spherical symmetry throughout the test. This can only occur if the diffusive residence times (i.e., mass (τ_m) and thermal (τ_k) are much lower than the buoyancy-controlled residence time (τ_b). Using the droplet diameter (D) as the characteristic length the expressions for the ratio of these two characteristic times to the buoyancy controlled residence time are

$$\frac{\tau_k}{\tau_b} = \frac{\sqrt{g\,D^3}}{\alpha_g} \tag{7}$$

and

$$\frac{\tau_m}{\tau_b} = \frac{\sqrt{g\,D^3}}{\mathcal{D}_g} \tag{8}$$

where α_g and $\mathcal{D}_g$ are the thermal and mass diffusivies of the gas phase. In order to justify neglecting buoyant effects the above ratios must be much lower than unity. This is only accomplished by changing at least one of the three independent variables, droplet diameter, pressure or gravity level (or some combination of the three).

Experiments in 1-g environments, performed in pressures of 1 atmosphere, require droplet diameters substantially smaller than 1 mm, smaller than the cool flame extinction droplet diameters. In addition, the FLEX experiments show the importance of radiative hot-flame extinction in establishing the cool flame. This can only be achieved in true microgravity experiments. Aircraft experiments (g-levels on the order of $10^{-2} - 10^{-3} g_0$) cannot reliably produce radiative extinction and neither drop tower nor aircraft experiments have the reduced-gravity times necessary to observe hot-flame extinction, quasi-steady cool flame burning and cool flame extinction.

Since diffusivities are inversely proportional to pressure the residence time ratios could alternatively be reduced by reducing test pressures. Chung and Law (1986) used this approach to measure extinction droplet diameters and from that determine single step chemical kinetic constants for decane in normal gravity. The range of oxygen concentrations and pressures was, however, very limited and the authors could only study diffusive extinction, not radiative extinction. Studying such a small range of droplet diameters, pressures and oxygen concentrations would severely limit the ability to achieve the stated objectives of the present study. Furthermore, Easton (1998) showed that the conditions that yielded finite extinction diameters in the work of Chung and Law (1986) burned to completion (no flame extinction) in microgravity. The author attributed this to a small residual buoyant-flow that is large enough in the vicinity of the flame to influence the extinction process (Struk et al., 1997).

The need for extended duration microgravity facilities is predicated on the fact that the burn-to-completion time for large droplets is longer than the time available in the ground-based facilities. Typically the droplet life-time (τ_l) can be estimated from the initial droplet size (D_0) and the average burning rate constant (k) as $\tau_l = \frac{D_0^2}{k}$. The values of τ_l for n-heptane, and methanol droplets burning in air at one atmospheric pressure range from 18 to 72 s for initial droplet diameters in the range 3 to 6 mm assuming an average burning rate constant of 0.5 mm^2/s. Moreover, high fidelity experiments demand additional microgravity time for droplet deployment, droplet quiescence, and ignition. Experiments involving radiative extinction require that the droplets be ignited in microgravity. Both Dietrich et al. (2005) and Easton (1998) studied extinction of single

droplets in drop towers. Dietrich et al. (2005) used the Japan Microgravity Center 10 s drop tower, a facility no longer available, and even then could only study a limited parameter space because of the limited microgravity time. It is quite likely that cool flames were present in some of the experiments. Their presence was likely only momentary as the test ended shortly after hot-flame extinction, so only a very short period (1 sec) of cool flame burning and no cool flame extinction could be observed. Therefore, the only facility which will enable data of sufficient quality over a wide parameter space is the microgravity environment available in extended-duration microgravity facilities (i.e. the ISS).

5 Science Requirements

5.1 Experiment Requirements

This section describes the experimental requirements and the rationale behind the requirements. A summary of all the requirements is provided in tabular form is first, followed by a more detailed explanation about the rationale behind the requirement.

Table 1: Hardware requirements tabulation.

Section	Description	Requirements
5.1.1	Test Fuels	- see list below - research grade, dry, degassed, highest purity commercially available - fuel temperature at the start of the test shall be in the range of 18 - 27 C
5.1.2	Droplet Deployment and Ignition	- 2 mm to 6 mm $\pm$ 0.25 mm and reproducible to within $\pm$ 10% - support fiber diameter $\leq$ 40 μm - hotwire ignition with selectable power and duration - igniter positioning shall be approximately 1-5 droplet radii away from surface, command controllable to within 0.5mm, and removable from the field of view - a spherical zone of exclusion at least $10D_0$ with the center located at the deployment site
5.1.3	Initial Pressure	- test pressures at 0.5 - 3.0 (5.0, desired) atm $\pm$ 0.05 atm - chamber pressure to be maintained within $\pm$ 10% of initial conditions throughout each test.
5.1.4	Initial Gas Composition	- mole fractions of O_2 from 0.10 to 0.40 - mole fractions of N_2, CO_2, He and Xe from 0 to 0.9 - tolerance on initial charge is $\pm$ 0.005 for O_2, $\pm$ 0.01 for N_2, He, Xe and CO_2.
5.1.5	Misc. Ambient Requirements	- initial gas temperature at 18 - 27 C - humidity $<$ 10% - quiescent atmosphere prior to ignition - well-mixed gases prior to ignition.
5.1.6	Operational Requirements	- allow at least 2 minutes after filling chamber to ensure gas temperature and pressure has stabilized - allow a 'droplet dwell time' of at least 10 sec to ensure all droplet motion imparted by droplet deployment and needle retraction has subsided - a 'near real time' downlink of the color camera video and the chamber gas pressure and temperature shall be provided - fuel vapor mole fraction of $<$ 0.005 in the atmosphere - for chamber atmospheres that do not use CO_2 as a diluent the atmosphere shall consist of $<$ 0.02 mole fraction (for each species) CO, CO_2 , and other products

5.1.7	Microgravity Requirements	-acceleration levels are required to be $2x10^{-6} - 2x10^{-4}$ on three axes depending on the size of the droplet - measurement accuracy shall be $1x10^{-6}$ - frequency range shall be $0.01 - 125\,Hz$ - sampling rate shall be $2 - 5$ times the frequency

5.1.1 Test Fuels

In order to further our understanding of the low temperature burning regime (Objective 1), we propose an extensive study of n-dodecane.

To study the effect of isomeric structure and fuel composition (Objective 2), we propose to study practical fuel additives and components 2,6,10 trimethyldodecane (farnescane) and 2,2,4,6,6 pentamethylheptane both as pure liquid droplets and mixtures of these fuels with n-dodecane.

To study the relationship between the cool flame droplet burning characteristics and fuel Octane and Cetane numbers we propose to study Primary Reference Fuel mixtures (PRF) of n-heptane and 2,2,4 trimethylpentane (iso-octane) and Toluene Reference Fuel (TRF) mixtures that have octane numbers of 50, 70 and 90.

As a final study related to Objective 2, we propose to study a Jet A surrogate mixture fuel that is a mixture of n-dodecane, iso-octane, n-propyl benzene and 1,3,5 trimethyl benzene.

To study the effect that fuel additives have on suppressing the low temperature burning behavior of droplets (Objective 3), we propose to study mixtures of n-dodecane and di-tertiary-butyl-peroxide.

The complete fuel list in order of priority follows.

Fuel Type:

1. n-dodecane
2. 2,6,10 trimethyldodecane (farnesane)
3. n-dodecane/2,6,10 trimethyldodecane mixtures (3 mixtures ea.)
4. n-dodecane/2,2,4,6,6 pentamethylheptane mixtures (3 mixtures ea.)
5. n-dodecane/iso-octane/n-propyl benzene/1,3,5 trimethyl benzene (2 mixtures ea.)
6. n-heptane/2,2,4 trimethylpentane mixtures
7. 2,2,4,6,6 pentamethylheptane (this fuel is for ground-based testing only)
8. n-dodecane/di-tertiary-butyl-peroxide mixtures (this mixture is for ground-based testing only)

Fuel Purity: purity levels shall be the highest purity level that is commercially available (research grade). Liquids shall be degassed and contain the lowest water content commercially available.
Quality Assurance: certification of test samples shall be provided prior to flight
Fuel Temperature: in the range of 18 - 27 C prior to the start of any test.

5.1.2 Droplet Deployment and Ignition

Droplet size during the experiments will vary between 2 mm and 6 mm. The droplets will either be free-deployed (no support) or supported on a thin fiber to minimize droplet motion. Hot-wire igniters positioned at the proper location before deployment ignite the droplet. Following deployment, after a preset dwell time (to allow droplet surface oscillations to decay to acceptable levels), the hot-wire igniters ignite the droplet (using a minimal amount of energy) and then de-energize and withdraw a minimum of 10 droplet diameters away from the droplet.

Droplet size: droplet diameter shall vary from $2\,mm$ to $6\,mm \pm 0.25\,mm$
Droplet reproducibility: droplet size shall be reproducible to within $\pm\,10\%$
Support fiber: support fiber diameter shall be less than or equal to $40\,\mu m$
Droplet Ignition: hot-wire ignition
Igniter Positioning: igniter tip shall be positioned within $0.5 - 2.5\,D_0$ away from the anticipated droplet surface. The position of igniter tip shall be controllable by command to within $0.5\,mm$. The igniter tip shall be removed from viewing area upon ignition.
Igniter operation: the power level and duration of igniter operation shall be controllable by command in order to provide the ability to ignite droplet with the minimum ignition energy necessary to sustain combustion.
Zone of exclusion: a spherical zone of exclusion centered at the droplet deployment and extending a minimum of 10 droplet diameters (initial) will be free from any solid objects except for the fiber when it is in use.

5.1.3 Initial Pressure

The ambient pressure strongly influences the low temperature burning behavior of the droplet.

Ambient pressure: initial ambient absolute pressure shall be set to $0.5 - 3.0\,atm$ (necessary), $0.5 - 5.0\,atm$ (desired) $\pm\,0.05 atm$.
Pressure transient:: chamber pressure shall be $\pm\,10\%$ of the initial ambient pressure throughout each test.

5.1.4 Initial Ambient

The ambient oxygen mole fraction influences the burning rate, extinction diameter, flame chemistry and flame characteristics (size, temperature). This parameter will vary from 0.4 down to the limit where no flame can be sustained at any droplet diameter. The ambient inert gases vary the thermo-physical properties of the ambient and thus vary the characteristic chemical times of both the hot and cool flames. This enables variation of the hot and cool flame extinction diameters over a wide range to better test and validate theoretical and numerical models.

Oxygen Mole Fraction: oxygen mole fraction shall range from $0.1 - 0.4 \pm 0.005$.
Ambient Gas Type: N_2, CO_2, He, Xe, and mixtures thereof.
Ambient Gas Composition: the exact ambient gas composition will be determined prior to each test day (not to exceed the ambient oxygen mole fractions in the range above), but will involve binary (oxidizer plus one inert) and possibly ternary (oxidizer plus two inerts) mixtures.

5.1.5 Misc. Ambient Requirements

Ambient Quiescience: gases shall be well-mixed and quiescent prior to ignition.
Ambient temperature: initial chamber gas temperature shall be $18 - 27\,C$.
Relative humidity: chamber relative humidity shall be less than 10%.

5.1.6 Operational Requirements

The chamber shall be filled with the appropriate atmosphere, which depending on the test point, will vary in pressure from 0.5 atm to 5.0 atm, and vary in O_2 concentration from 0.1 to 0.4 mole fraction, with different inert gases and gas mixtures. A settling time of approximately 2 minutes will elapse prior to initiating the test in order to ensure that the temperature and pressure of the chamber gases have stabilized. A test proceeds by dispensing a pre-determined amount of fuel slowly 'stretching' the droplet and then rapidly retracting the needles to 'deploy' the droplet (either into the quiescent gas mixture or onto the fiber). The igniters, which are positioned close to the droplet, will then energize and ignite the droplet after which they will retract away from the droplet. All of the parameters (the igniter and needle position, fuel volume dispensed, dwell and ignition times) should be adjustable from the ground in near real-time during a test.

Gas stabilization time: allow at least 2 minutes after filling chamber to ensure that the chamber gas temperature and pressure has stabilized.
Real time downlink: a 'near real time' downlink of the color camera video and the chamber gas, pressure and temperature shall be provided.
Chamber Purity: fuel vapor mole fraction of < 0.005 in the atmosphere; < 0.02 mole fraction (each species) of CO, CO_2 and other products (except for CO_2 for tests in ambient environments with enriched CO_2). *Droplet dwell time:* the hardware shall allow a ground-controllable time between dispense and deployment and between deployment and ignition of up to 10 *sec*.

5.1.7 Microgravity Requirements

In order to compare the experimental data with theoretical results obtained under the conditions $Re \sim O(1)$ we need to minimize the effects of buoyancy on the flow field. The dimensionless parameter that compares the buoyancy effects to forced flow effects is the ratio of two dimensionless groups, the Gr/Re^2, where Gr is the Grashof number, and Re is the Reynolds number. The magnitude of this dimensionless group indicates the relative effect of buoyancy compared to forced convection and we need $Gr/Re^2 << 1$ in our experiments. This criterion can be translated into a requirement on the g-level as follows:

$$\frac{Gr}{Re^2} = \frac{g\,\beta\,\Delta T\,D}{U_\infty^2} << 1 \tag{9}$$

where g is the gravitational acceleration, β is the coefficient of thermal expansion, ΔT is the characteristic temperature difference, D is the characteristic length scale and U_∞ is the free-stream velocity. For the worst case scenario $\Delta T \sim 5$, $D \sim 1\,cm$ and $U_\infty \sim 1\,cm/s$ which yields a g/g_0 value of $1x10^{-5}$ as the required g-level (g_0 is the earth normal gravity).

Micro-gravity levels: accelerations are required to be less than $10^{-5}\,m/s^2$ in order to ensure buoyant forces are negligible.

5.2 Diagnostic Requirements

This section describes the diagnostic requirements and the rationale behind the requirements. A summary of all the requirements is provided in tabular form is first, followed by a more detailed explanation about the rationale behind the requirement.

Table 2: Diagnostic requirements tabulation.

Section	Description	Requirements
5.2.1	Droplet Imaging	- focal plane parallel to support fiber - FOV at least 3.0 cm (5.0 cm, preferred) centered on droplet (center of FOV) - resolution of 50 μm for smallest droplet size over entire FOV - frame rate at least 30 fps - depth of view at least 3.0 cm - ability to backlight the droplet
5.2.2	OH^* or CH Flame Imaging	- FOV at least 8.0 cm (10.0 cm, preferred) centered on droplet (center of FOV) - color detection for wavelengths of 310 nm $\pm 5nm$ or 430 nm $\pm 5nm$ - resolution of 100 μm - frame rate at least 30fps - depth of view at least 8.0 cm - adjustable gain
5.2.3	CH_2O Cool-Flame Imaging	- FOV at least 10.0 cm centered on droplet (center of FOV) - resolution of 100 μm - wavelength between 390 and 490 nm - frame rate at least 30 fps - depth of view at least 5.0 cm - adjustable gain, sensitivity to image cool flame
5.2.4	Color Flame Imaging (Experiment Monitoring Camera)	- FOV at least 5.0 cm and positioned such that entire flame is imaged - resolution of 100 μm - frame rate at least 30 fps - depth of view at least 5.0 cm - zoom capability requested - near real-time downlink
5.2.5	Flame Radiation	- radiometer used to detect water vapor radiation shall be filtered to detect wavelengths in within the spectral range of $6.0 - 6.5\,\mu m$ - radiometer used for broad-band radiation shall detect wavelengths within a band from $0.6 - 5.0\,\mu m$ - sample rate shall be at a frequency of 20 Hz - radiometers shall be positioned at least 15 cm from the droplet to enable detection of all incident radiation from the flame. - accuracy 5% of full scale incident radiation - response time constant to be $< 50\,ms$ - detect flame radiance in the 0.10 - 100 W range - field of view shall be at least 90 mm diameter centered around the deployment site

5.2.6	Fiber Temperature (desired)	- FOV at least 5 cm about the center of the deployed droplet - at least 2 fps - resolution of 100 μm over the entire FOV - detect fiber temperatures in the range 600 - 1500 K
5.2.7	Ambient Pressure and Temperature Measurement	- minimum sample rate shall be at 10 Hz - temperature accuracy shall be at least $\pm\, 0.5\, C$ in the range of $18 - 27\, C$ - pressure accuracy shall be at least $\pm\, 0.01\, atm$ in the range of $0.5 - 3\, atm$
5.2.8	Time Synchronization	- all measurements shall be referenced to GMT with a minimum accuracy of $\pm\, 0.03\, sec$

5.2.1 Droplet Imaging

A back-lit view of the droplet shall be provided that will allow accurate measurements of the droplet size as a function of time. This is necessary to obtain droplet burning rates and extinction droplet diameters. This view also yields quantitative regarding the soot shell and soot shell dynamics. The time resolution is necessary to accurately measure the burning rate constant and it's temporal variation as well as accurate measurements of the extinction droplet diameter. Experience during the FLEX experiments shows that the approximately 3.0 cm field-of-view (FOV) is acceptable. For freely deployed droplets, however, the success rate increases with increasing FOV size (the droplet does not drift out of the FOV). The CFI team therefore desires a larger FOV (but at the same spatial resolution.

Field of view: minimum of 3.0 cm centered about the droplet, 5.0 cm preferred
Resolution: 50 μm over the entire FOV.
Minimum frame rate: 30 fps over the duration of the test.
Focal Plane: the focal plane shall be parallel to the fiber.
Depth of Field: a depth-of-field of at least 3.0 cm.
Backlight: the ability to backlight the droplet image

5.2.2 $OH*$ or CH Hot-Flame Imaging

The flame structure and its dynamic response shall be obtained from flame imaging oriented perpendicular to the stream-wise flow direction. The flame image shall be derived from the ultraviolet OH-radical chemiluminescence or CH-radical emission intensity. This technique is well understood and has been implemented in a previous flight experiment (DCE) and the current FLEX experiments.

Field of view: minimum of 8.0 cm, 10.0 cm (desired)
Depth of view: minimum 3.0 cm, 5.0 cm (desired)
Color: shall detect wavelengths of 310 nm $\pm$ 5nm or 430 nm $\pm$ 5nm using an intensified camera in order to detect $OH*$ or CH radical emission, respectively.
Resolution: 100 μm (i.e. $>$ 5 lp/mm) over the entire FOV.
Minimum frame rate: 30 fps over the duration of the test.

Gain setting: shall be adjustable prior to each test.

5.2.3 CH_2O Cool-Flame Imaging

The biggest weakness of the FLEX testing to date involving cool flames is, with the notable exception of the narrowband radiometer on later tests, the absence of any to detect the cool flame. The cool flame is significantly less luminous than the hot flame which near extinction is near the lower limit of detectability with the existing camera systems. The proposed tests require the ability to image the cool flame. The theoretical and numerical analyses of the FLEX tests, in addition to ground-based work on cool flames, indicates that the cool flames have a relatively strong chemiluminescence from excited formaldehyde (CH_2O). Sheinson and Williams (1973) showed that cool flames emit visible light in the range of 350 - 500 nm (Figure 11).

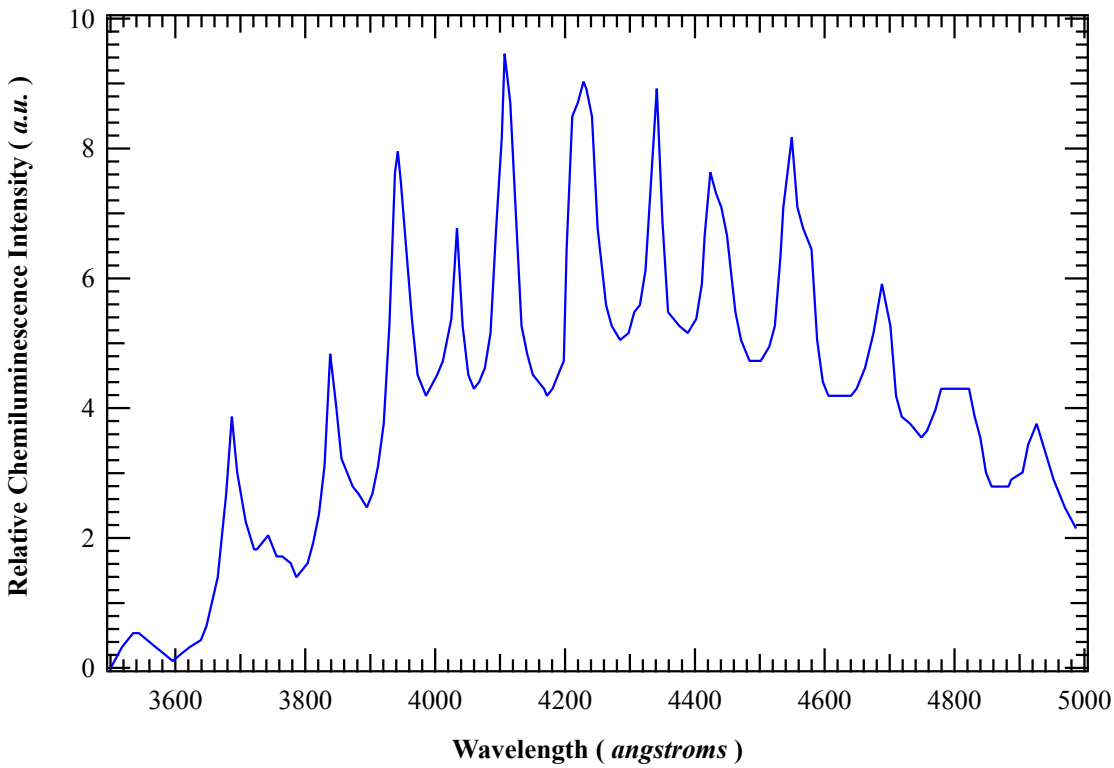

Figure 11: Chemiluminescence spectra from excited formaldehyde (Sheinson and Williams, 1973).

Field of view: minimum of 8.0 cm, 10.0 cm (desired)
Depth of view: minimum 3.0 cm, 5.0 cm (desired)
Color: shall detect wavelengths between approximately 390 nm and 490 nm using an intensified camera in order to detect CH_2O emission.
Resolution: 100 μm (i.e. $>$ 5 lp/mm) over the entire FOV.
Minimum frame rate: 30 fps over the duration of the test.
Gain setting: shall be adjustable prior to each test. Must have sufficient sensitivity to detect the

cool flames.[3]

5.2.4 Secondary Color Flame Imaging

A color CCD camera viewing the droplet at a specified angle will provide flame color information during combustion. Based on earlier flight experiments, it is also desired that this camera serve as the experiment's monitor camera to facilitate experiment operation/monitoring from the ground.

Orientation: the camera shall provide viewing of the droplet dispensing and deployment sequence in addition to providing a color camera view of the burning droplet.
Field of view: minimum of 5.0 cm
Depth of view: minimum of 5.0 cm
Resolution: 100 μm (i.e. $> 5\, lp/mm$) over the entire FOV.
Minimum frame rate: 30 fps over the duration of the test.
Downlink: image shall be down-linked in *near real-time* during each test.
Zoom: request the capability to 'zoom' (decreased FOV) this view for a more detailed view of the droplet formation and deployment processes during PI-selected tests.

5.2.5 Flame Radiation

The FLEX experiments to date have established the utility of flame radiometric measurements. The FLEX broadband radiometer captures the total flame radiation during the hot and cool flame. The gain on the radiometer, however, is fixed and set to capture the hot flame. While the radiometer does detect the cool flame, the cool flame radiance is very close to the lower limit of detection. As a result, the reading has a lower signal to noise ratio (accuracy less than the requirement in the original SRD in the cool flame region) than desired and cannot reliably detect cool flame extinction. For this program we require a broadband flame radiance measurement for both the hot flame and the cool flame. These measurements will be used to obtain the total radiant energy loss as well as to establish the exact moment of both cool and hot flame extinction and to supplement other imaging data in determining transient flame behavior.

Thermopile radiometers, positioned at distances far enough from the droplet to allow full view of the flame, can measure *broad-band* radiation and water-vapor radiation from the flame zone.

Water vapor: radiometer used to detect water vapor radiation shall be filtered to detect wavelengths within the spectral range of $6.0 - 6.5\, \mu m$)
Broad-band spectrum: radiometer used for broad-band radiation shall detect wavelengths within a band from $0.6\, \mu m - 5\, \mu m$.
Sample rate: data sampled from the radiometer shall be at a frequency of at least 20 Hz.
Positioning: radiometers shall be positioned at least 10 cm from the droplet to enable detection of all incident radiation from the flame.
Flame Radiance: detect flame radiancce between 0.10 and 100 W
Field of view: at least 90 mm centered on the deployment site
Response Time: The time constant of both the narrow band and broad band radiometers shall be less than 100 ms
Accuracy: 5% of full scale incident radiation

[3]The science team will work with the engineering team to verify this requirement.

5.2.6 Fiber/Flame Temperature

We *desire* to quantify the hot and cool flame temperature by measuring the broadband temperature of the SiC support fiber. Using the HiBMS-2 equipped with the Liquid Crystal Tunable Filter (LCTF) the FLEX experiments demonstrated the capability to estimate the hot-flame temperature from SiC emission during fiber supported tests. Ideally this was supposed to involve two color pyrometry using the HiBMS-2 with the LCTF cycling between two different wavelength bands. In practice, however, the cycling rate of the LCTF coupled with the poor transmission of the LCTF and the quantum efficiency (QE) of the detector precluded estimating fiber/flame temperature using this method. Using the HiBMS-2 and LCTF at a fixed wavelength (optimizing the QE/LCTF response) allowed an estimate of the flame temperature during the hot flame.

The HiBMS-2/LCTF combination, however, cannot measure the fiber/flame temperature during the cool flame. If the LCTF is replaced by a fixed filter and the HiBMS-2 signal can be integrated over a longer period of time, it may be possible to get a signal sufficient to estimate the fiber/flame temperature during the cool flame. An estimate of the cool flame temperature would be invaluable.

Orientation: camera shall provide full view of the droplet and the flame.
Frame Rate: frame rate shall be at least 2 fps
Field of View: the FOV shall be at least $5.0\,cm\,x\,5.0\,cm$ about the center of the deployed droplet
Temperature Range: the camera shall estimate the fiber temperature in the 600 - 1500 K range (not necessarily over the entire range within the same test, but user selectable)
Resolution: $100\,\mu m$ (i.e. $>\ 5\,lp/mm$) over the entire FOV.

5.2.7 Ambient Temperature and Pressure Measurement

During each test the chamber gas temperature and pressure measurements shall be required. The following are the specifications for this data.
Sample rate: minimum sample rate shall be at 10 Hz
Temperature: accuracy shall be at least $\pm\,0.5\,C$ in the range of 18 - 27 C.
Pressure: accuracy shall be at least $\pm\,0.01\,atm$ in the range of 0.50 - 5.0 atm.

5.2.8 Synchronization

Experiment objectives require all data to be time-synchronized to a reference time. This will allow accurate interpretation of the data and evaluate droplet regression rate, flame structure, and flame extinction as a function of time.
Time synchronization: all measurements shall be referenced to GMT with a minimum accuracy of $\pm\,0.03\,sec$.

6 Test Matrix and Experiment Procedure

6.1 Flight Experiment Test Procedures

The proposed CFI experiments involve igniting and observing the burning behavior of relatively large droplets. The experiments seek to observe the ignition, hot-flame burning and flame extinction, cool flame initiation and burning and finally, cool flame extinction of primarily free-floated fuel droplets in q quiescent ambient envrionment. The Science Definition Team will work with the engineering team to determine the optimal order for the experiments. The order is based partially on experiment priority (e.g., it may be important to perform some tests first), hardware considerations (e.g., the fuel system operates better if the tests run in increasing ambient pressure) and resource optimization. Based on the experience with the FLEX experiments, the experiment sequence on a given test day proceeds as follows:

1. Select the ambient environment for the tests. This will be done several months before testing and changes can be made up to 72 hours before the test day (changes to diluent may require additional lead time for on-orbit bottle change-outs).

2. Perform the Fuel-Oxidizer Mixing Apparatus (FOMA) operations to set the test ambient. This will be done immediately prior to testing.

3. Perform a droplet combustion test by completing the following operations in approximate order.

   (a) Position the igniters, fiber and needles and prepare the diagnostics for data acquisition.
   (b) Open the fuel valve and begin dispensing fuel.
   (c) Dispense the appropriate fuel volume for a given droplet size (this can be changed in near real-time) using the downlink video view to guide the test.
   (d) Zoom the downlink video view out to observe droplet combustion test.
   (e) Run the automated sequence which consists of the following steps.
      i. Turn the chamber lights off.
      ii. Start data recording on all cameras and radiometers.
      iii. Rapidly retract the needles to *deploy* the droplet.
      iv. Power the igniters (they will turn off and retract after a preset period of time).
      v. Observe the droplet burning on the real-time video (recording locally at the Telescience Support Center, TSC) until the test is complete and on-orbit video recording stops after a preset period of time.
      vi. Run the circulation fan for approximately 15 seconds to mix the contents of the chamber.

4. Determine the success of the test and whether to save the on-orbit video files. On-orbit storage is limited and unsuccessful tests (e.g., no ignition) need to be deleted to save storage space.

5. Repeat step 3 TBD times (typically 5 - 10) for a range of droplet sizes.

After completing the tests on a given test day, the on-orbit will be downlinked to the ground and transferred to the TSC. There the data is de-compressed and provided to the SDT for detailed analysis. This process typically takes 3 to 7 days. This process is then repeated for each desired test atmosphere.

6.2 FLEX Test Matrix

The proposed test matrix is fashioned so as to meet the stated science objectives and at the same time meet the constraints imposed by the hardware as well as the safety requirements of space experiments. The tables below detail the proposed tests. These test matrices, however, are primarily intended to be a guide to overview the proposed testing and allow the engineering team to make the appropriate resource estimates. The exact test matrix will evolve as we perform more detailed analyses of the FLEX data and perform additional FLEX-2 tests. The SDT also expects to make changes to the test matrices as CFI testing proceeds and the results from downlinked tests gets analyzed (i.e. using previous tests to guide future tests rather than marching to a rigid test matrix).

Table 3 provides the envelope conditions for n-dodecane. This is the base fuel and has the most extensive test matrix. The ambient environment for these tests will include nitrogen, helium and xenon-diluted ambient environments at a range of ambient oxygen mole fractions and pressures.

Table 4 provides the envelope conditions for the other fuels and fuel mixtures. The ambient environment for these tests will be oxygen and nitrogen mixtures over a range of ambient oxygen mole fractions and pressures.

Table 3: Nominal test matrix for n-dodecane. The droplet size range for the tests is 2 - 6 mm.

n-dodecane			
$P\ (atm)$	Y_{O2}	Diluent	Tests
1.0	0.21 0.18 0.15	N_2	10
0.50	0.21	N_2	5
0.75			5
1.5			5
2.0			10
3.0			5
4.0			10
5.0			10
1.0	0.21 0.25 0.30	He	5 5 5
0.75	0.21	He	5
3.0			5
5.0			5
1.0	0.21 0.18 0.15	Xe	5 5 5
0.50	0.21	Xe	5
2.0			5
3.0			5

Table 4: Nominal test matrix for the other fuels and fuel mixtures. The droplet size range for the tests is 2 - 6 mm.

2,6,10 trimethyldodecane n-dodecane/2,6,10 trimethyldodecane - 3 mixtures n-dodecane/2,2,4,6,6 pentamethylheptane - 3 mixtures n-dodecane/iso-octane/n-propyl benzene/1,3,5 trimethyl benzene - 2 mixtures n-heptane/2,2,4 trimethylpentane mixtures - 3 mixtures			
P (atm)	Y_{O2}	Diluent	Tests
1.0	0.21 0.18 0.15	N_2	10
0.50			5
0.75			5
1.5			5
2.0	0.21	N_2	10
3.0			5
4.0			10
5.0			10

7 Success Criteria

7.1 Minimal Success

- Obtain droplet diameter and either $OH*/CH$ color video hot-flame measurements as function of time for n-dodecane over a range of pressures spanning 0.5 - 3.0 atm (minimum of four pressure conditions) and at least two ambient oxygen mole fractions and two diluent gases for a range of droplets that exhibit cool flame burning and cool-flame extinction.

- Acquire droplet diameter and either $OH*/CH$ or color video flame measurements for four additional pure fuels and/or fuel mixtures identified in Table 4 over a range of pressures spanning 0.5 - 3.0 atm (minimum of four pressure conditions) and at least two ambient oxygen mole fractions for a range of droplets that exhibit cool flame burning and cool flame extinction.

- For the tests described above obtain hot-flame and cool-flame radiometric measurements.

- For the tests described above obtain a measure of the cool flame diameter.

7.2 Complete Success

- Obtain droplet diameter and either $OH*/CH$ color video hot-flame measurements as function of time for n-dodecane over a range of pressures spanning 0.5 - 5.0 atm (minimum of seven pressure conditions) and at least three ambient oxygen mole fractions and three diluent

gases for a range of droplets that exhibit cool flame burning and cool-flame extinction.

- Acquire droplet diameter and either $OH*/CH$ or color video flame measurements for seven additional pure fuels and/or fuel mixtures identified in Table 4 over a range of pressures spanning 0.5 - 5.0 atm (minimum of seven pressure conditions) and at least three ambient oxygen mole fractions for a range of droplets that exhibit cool flame burning and cool flame extinction.
- For the tests described above obtain hot-flame and cool-flame radiometric measurements.
- For the tests described above obtain a measure of the cool flame diameter.

8 Data Requirements

The primary scientific data obtained during these experiments will be the time histories of droplet diameter, flame shape, and radiant energy output by the flame. All of the data from the flight experiment will be stored and archived electronically in an open-source format and be publicly available. This includes scientific image and radiometric data as well as housekeeping data such as chamber temperature, pressure, etc. The GRC investigators will be responsible for archiving the raw and analyzed experimental data.

In addition, pending available resources, the Science Definition Team expects to analyze the flight data as detailed below both during and after the completion of the experiment. That data will also be in an open source data format and be made publicly available.

8.1 Temporal Droplet History

The measurement of the droplet history comes from the recorded backlit image data by measuring the size of the droplet as a function of time before and after ignition. The droplet burning rate and extinction droplet diameter are derived from this data. The archived data will include the raw images from the CIR camera along with the camera settings, illumination package details and scale factors. Additional archived data will include, at a minimum, analyzed data of the equivalent droplet size as a function of time, the initial and extinction droplet sizes, droplet shape (for fiber supported droplets).

8.2 Flame Shape and Structure

Two cameras provide flame images as a function of time, the $OH*/CH$ and CH_2O images and the view from a color CCD camera. There is a large amount of data derived from these views including, but not limited to flame size and shape as a function of time, radial $OH*$ profiles (Marchese et al., 1996), flame luminosity and color (qualitative measures of soot formation/destruction) as functions of time, and the time of flame extinction. Accurate measurements require that the flame be in focus and that appropriate scale factors are available. The archived data will include the raw images from all of the cameras along with all of the camera settings and calibrations, and scale factors.

8.3 Flame Radiation

Data obtained from both the wide and narrow band radiometers will be used to measure the non-luminous flame radiation. Accurate measurements require calibrated radiometers with well-defined spectral characteristics. In order to be useful in extracting extinction information and obtain ratios of radiative heat loss to combustion heat release, the data must be accurately time stamped and correlated with the flame, droplet and soot image data. The archived data will include the raw radiometer data, the calibration factors and view factor information (geometry of the radiometer relative to the droplet). Analyzed data will include, at a minimum, the flame radiance as a function of time (time-stamped to the video data).

9 Principal Deliverables

The science team at GRC, under the direction of the SDT will process and archive all of the downloaded data mentioned in the previous section.

References

Banu, B. (2008). Fluids and combustion facility (FCF) and combustion integrated rack (CIR). Payload Accomodations Handbook CIR-DOC-4064, NASA John H. Glenn Research Center, Cleveland, Ohio.

Biet, J., Hakka, M. H., Warth, V., Glaude, P.-A., and Battin-Leclerc, F. (2008). Experimental and modeling study of the low-temperature oxidation of large alkanes. *Energy & Fuels*, 22(4):2258–2269.

Buda, F., Bounaceur, R., Warth, V., Glaude, P.-A., Fournet, R., and Battin-Leclerc, F. (2005). Progress toward a unified detailed kinetic model for the autoignition of alkanes from c_4 *to* c_{10}between 600 and 1200 k. *Combustion and flame*, 142(1):170–186.

Card, J. and Williams, F. (1992a). Asymptotic analysis of the structure and extinction of spherically symmetrical n-heptane diffusion flames. *Combustion science and technology*, 84(1-6):91–119.

Card, J. and Williams, F. (1992b). Asymptotic analysis with reduced chemistry for the burning of n-heptane droplets. *Combustion and flame*, 91(2):187–199.

Chao, B., Law, C., and T'ien, J. (1991). Structure and extinction of diffusion flames with flame radiation. volume 23, pages 523–531. Elsevier.

Chaos, M. and Dryer, F. L. (2008). Syngas combustion kinetics and applications. *Combustion Science and Technology*, 180(6):1053 – 1096.

Chaos, M., Kazakov, A., Zhao, Z., and Dryer, F. L. (2007). A high-temperature chemical kinetic model for primary reference fuels. *International Journal of Chemical Kinetics*, 39(7):399–414.

Choi, M. Y. and Dryer, F. L. (2001). Microgravity droplet combustion. *Microgravity Combustion: Fire in Free Fall, Combustion Treatise*, pages 183–297.

Chung, S. H. and Law, C. K. (1986). An experimental study of droplet extinction in the absence of external convection. *Combustion and Flame*, 64:237–241.

Cuoci, A., Frassoldati, A., Faravelli, T., and Ranzi, E. (2013). Cool flames in droplet combustion. *XXXVI Meeting of the Italian Section of the Combustion Institute*.

Cuoci, A., Mehl, M., Buzzi-Ferraris, G., Faravelli, T., Manca, D., and Ranzi, E. (2005). Autoignition and burning rates of fuel droplets under microgravity. *Combustion and Flame*, 143(3):211 – 226.

Curran, H., Gaffuri, P., Pitz, W., and Westbrook, C. (1998). A comprehensive modeling study of n-heptane oxidation. *Combustion and Flame*, 114(1–2):149 – 177.

Curran, H. J., Gaffuri, P., Pitz, W., and Westbrook, C. (2002). A comprehensive modeling study of iso-octane oxidation. *Combustion and flame*, 129(3):253–280.

Davidson, D., Haylett, D., and Hanson, R. (2008). Development of an aerosol shock tube for kinetic studies of low-vapor-pressure fuels. *Combustion and Flame*, 155(1):108–117.

Dembia, C. L., Liu, Y. C., and Avedisian, C. T. (2012). Automated data analysis for consecutive images from droplet combustion experiments. *Image Analysis and Stereology*, 31:137 – 148.

Dietrich, D. L., Haggard Jr, J. B., Dryer, F. L., Nayagam, V., Shaw, B. D., and Williams, F. A. (1996). Droplet combustion experiments in spacelab. In *Symposium (International) on Combustion*, volume 26, pages 1201–1207. Elsevier.

Dietrich, D. L., Struk, P. M., Ikegami, M., and Xu, G. (2005). Single droplet combustion of decane in microgravity: Experiments and numerical modeling. *Combustion Theory and Modeling*, 9(4):569–585.

Easton, J. W. (1998). Large diameter, radiative extinction experiments with decane droplets in microgravity. Master's thesis, Case Western Reserve University, Cleveland, Ohio 44106.

El Bakali, A., Delfau, J.-L., and Vovelle, C. (1999). Kinetic modeling of a rich, atmospheric pressure, premixed n-heptane/o¡ sub¿ 2¡/sub¿/n¡ sub¿ 2¡/sub¿ flame. *Combustion and flame*, 118(3):381–398.

Faeth, G. (1977). Current status of droplet and liquid combustion. *Progress in Energy and Combustion Science*, 3(4):191–224.

Fairlie, R., Griffiths, J., Hughes, K., and Pearlman, H. (2005). Cool flames in space: experimental and numerical studies of propane combustion. *Proceedings of the Combustion Institute*, 30(1):1057–1064.

Farouk, T. I. and Dryer, F. L. (2014). Isolated n-heptane droplet combustion in microgravity: "Cool Flames - Two-stage combustion ". *Combustion and Flame*, 161(2):565 – 581.

Farouk, T. I., Hicks, M. C., and Dryer, F. L. (2014). Multistage oscillatory "cool flame" behavior for isolated alkane droplet combustion in elevated pressure microgravity condition. *Proceedings of the Combustion Institute*, 35:to appear.

Foster, M. R. and Pearlman, H. (2012). Non-isothermal cool flames in unstirred static reactors: A compressible model with global kinetics. *Microgravity Science and Technology*, 24(2):113–125.

Frank-Kamenetskii, D. A. and Thon, N. (1955). *Diffusion and heat exchange in chemical kinetics*. Princeton University Press Princeton.

Griffiths, J. (1995). Reduced kinetic models and their application to practical combustion systems. *Progress in Energy and Combustion Science*, 21(1):25–107.

Haas, F. M., Chaos, M., and Dryer, F. L. (2009). Low and intermediate temperature oxidation of ethanol and ethanol-PRF blends: An experimental and modeling study. *Combustion and Flame*, 156:2346 – 2350.

Haas, F. M., Ramcharan, A., and Dryer, F. L. (2011). Relative reactivities of the isomeric butanols and ethanol in an ignition qualitty tester. *Energy and Fuels*, 25:3909 – 3916.

Harper, M. R., Geem, K. M. V., Pyl, S. P., Marin, G. B., and Green, W. H. (2011). Comprehensive reaction mechanism for n-butanol pyrolysis and combustion. *Combustion and Flame*, 158:16 – 41.

Held, T., Marchese, A., and Dryer, F. (1997). A semi-empirical reaction mechanism for n-heptane oxidation and pyrolysis. *Combustion Science and Technology*, 123(1-6):107–146.

Jahangirian, S., Dooley, S., Haas, F. M., and Dryer, F. L. (2012). A detailed experimental and kinetic modeling study of n-decane oxidation at elevated pressures. *Combustion and Flame*, 159(1):30 – 43.

Kumagai, S. (1956). Combustion of fuel droplets in a falling chamber with special reference to the effects of natural convection. *Jet Propulsion*, 26(9):786–790.

Law, C. (1975). Aymptotic theory for ignition and extinction in droplet burning. *Combustion and Flame*, 24:89–98.

Law, C. K. (1982). Recent advances in droplet vaporization and combustion. *Progress in Energy and Combustion Science*, 8(3):171–201.

Marchese, A., Dryer, F., and Nayagam, V. (1999a). Numerical modeling of isolated n-alkane droplet flames: initial comparisons with ground and space-based microgravity experiments. *Combustion and Flame*, 116(3):432–459.

Marchese, A. J., Dryer, F. L., and Nayagam, V. (1999b). Numerical modeling of isolated n-alkane droplet flames: initial comparisons with ground and space-based microgravity experiments. *Combustion and Flame*, 116(3):432 – 459.

Marchese, A. J., Dryer, F. L., Nayagam, V., and Colantonio, R. O. (1996). Hydroxyl radical chemiluminescence imaging and the structure of microgravity droplet flames. *Proceedings of the Combustion Institute*, 26:1219–1226.

Naidja, A., Krishna, C., Butcher, T., and Mahajan, D. (2003). Cool flame partial oxidation and its role in combustion and reforming of fuels for fuel cell systems. *Progress in energy and combustion science*, 29(2):155–191.

Nayagam, V., Dietrich, D. L., Ferkul, P. V., Hicks, M. C., and Williams, F. A. (2012). Can cool flames support quasi-steady alkane droplet burning? *Combustion and Flame*, 159(12):3583 – 3588.

Nayagam, V., Haggard, J., Colantonio, R., Marchese, A., Dryer, F., Zhang, B., and Williams, F. (1998). Microgravity n-heptane droplet combustion in oxygen-helium mixtures at atmospheric pressure. *AIAA journal*, 36(8):1369–1378.

Pearlman, H. (2000). Low-temperature oxidation reactions and cool flames at earth and reduced gravity. *Combustion and flame*, 121(1):390–393.

Perkin, W. H. (1882). Some observations on the luminous incomplete combustion of ether and other organic bodies. *J. Chem. Soc., Trans.*, 41:363–367.

Peters, N., Paczko, G., Seiser, R., and Seshadri, K. (2002). Temperature cross-over and non-thermal runaway at two-stage ignition of n-heptane. *Combustion and Flame*, 128(1–2):38 – 59.

Prince, J. C. and Williams, F. A. (2012). Short chemical-kinetic mechanisms for low-temperature ignition of propane and ethane. *Combustion and Flame*, 159(7):2336–2344.

Ranzi, E., Frassoldati, A., Granata, S., and Faravelli, T. (2005). Wide-range kinetic modeling study of the pyrolysis, partial oxidation, and combustion of heavy n-alkanes. *Industrial & engineering chemistry research*, 44(14):5170–5183.

Ranzi, E., Gaffuri, P., Faravelli, T., and Dagaut, P. (1995). A wide-range modeling study of n-heptane oxidation. *Combustion and Flame*, 103(1):91–106.

Reitz, R. D. (2013). Directions in internal combustion engine research. *Combustion and Flame*, 160(1):1 – 8.

Ridler, T. W. and Calvard, S. (1978). Picture thresholding using an iterative selection method. *IEEE Transactions on Systems, Man, and Cybernetics*, SMC-8(8):230 – 232.

Robbins, J. and Shinn, C. (2010). Multi-user droplet combustion apparatus flex2. Reflight Safety Data Package MDC-DOC-1790A, NASA John H. Glenn Research Center, Cleveland, Ohio.

Schnaubelt, S., Moriue, O., Coordes, T., Eigenbrod, C., and Rath, H. J. (2000). Detailed numerical simulations of the multistage self-igniiton process of n-heptane isolated droplets and their verification by comparison with microgravity experiments. *Proceedings of the Combustion Institute*, 28:953–960.

Seiser, R., Pitsch, H., Seshadri, K., Pitz, W., and Gurran, H. (2000). Extinction and autoignition of¡ i¿ n¡/i¿-heptane in counterflow configuration. *Proceedings of the Combustion Institute*, 28(2):2029–2037.

Shaw, B. D., Clark, B. D., and Wang, D. (2001). Spacelab experiments on combustion of heptane/hexadecane droplets. *AIAA Journal*, 39(12):2327 – 2336.

Sheinson, R. S. and Williams, F. W. (1973). Chemiluminescence spectra from cool and blue flames: Electrnically excited formaldehyde. *Combustion and Flame*, 21:221 – 230.

Sirignano, W. A. (1983). Fuel droplet vaporization and spray combustion theory. *Progress in Energy and Combustion Science*, 9(4):291–322.

Smith, J. M., Simmie, J. M., and Curran, H. J. (2005). Autoignition of heptanes; experiments and modeling. *International journal of chemical kinetics*, 37(12):728–736.

Struk, P. M., Ackerman, M., Nayagam, V., and Dietrich, D. L. (1998). On calculating burning rates during fiber supported droplet combustion. *Microgravity Science and Technology*, XI/4:144–151.

Struk, P. M., T'ien, J. S., Dietrich, D. L., and d B Lenhert (1997). Experimental studies of flame shape around droplets in different buoyant environments. 35th Aerospace Sciences Meeting and Exhibit AIAA-97-1001, American Institute of Aeronautics and Astronautics.

Tanabe, M., Bolik, T., Eigenbrod, C., Rath, H., Sato, J., and Kono, M. (1996). Spontaneous ignition of liquid droplets from a view of non-homogeneous mixture formation and transient chemical reactions. In *Symposium (International) on Combustion*, volume 26, pages 1637–1643. Elsevier.

Tanabe, M., Kono, M., Sato, J., Koenig, J., Eigenbrod, C., Dinkelacker, F., and Rath, J. J. (1995). Two stage ignition of n-heptane isolated droplets. *Combustion Science and Technology*, 108:103–119.

Tanaka, S., Ayala, F., Keck, J. C., and Heywood, J. B. (2003). Two-stage ignition in hcci combustion and hcci control by fuels and additives. *Combustion and flame*, 132(1):219–239.

Wang, X.-j. and Mou, C. Y. (1985). A thermokinetic model of complex oscillations in gaseous hydrocarbon oxidation. *The Journal of chemical physics*, 83:4554.

Westbrook, C. K. and Dryer, F. L. (1981). Simplified reaction mechanisms for the oxidation of hydrocarbon fuels in flames. *Combustion science and technology*, 27(1-2):31–43.

Xu, G., Ikegami, M., Honma, S., Ikeda, K., Ma, X., Nagaishi, H., Dietrich, D. L., and Struk, P. M. (2003). Inverse influence of initial diameter on droplet burning rate in cold and hot ambiences: A themal action of flame in balance with heat loss. *International Journal of Heat and Mass Transfer*, 46:1155–1169.

Yang, C.-H. and Gray, B. F. (1969). Slow oxidation of hydrocarbons and cool flames. *The Journal of Physical Chemistry*, 73(10):3395–3406.